Aberrant cortex contractions impact mammalian oocyte quality

Elvira Nikalayevich, Gaëlle Letort, Ghislain de Labbey, Elena Todisco, Anastasia Shihabi, Hervé Turlier, Raphaël Voituriez, Mohamed Yahiatene, Xavier Pollet-Villard, Metello Innocenti, et al.

Short article

Developmental Cell

Aberrant cortex contractions impact mammalian oocyte quality

Graphical abstract

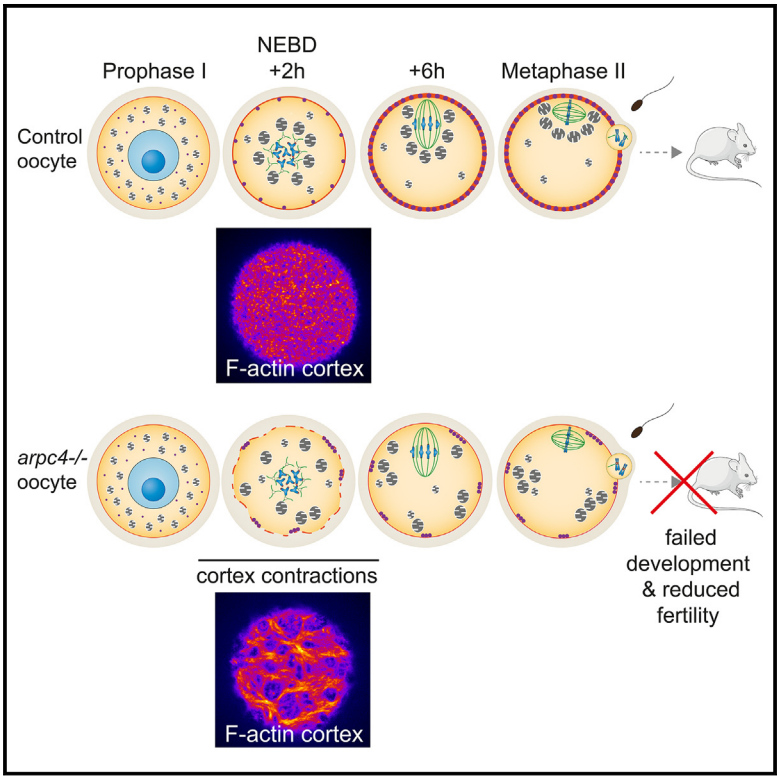

Highlights

- Mouse oocytes depleted of Arp2/3 complex re-organize their cortex upon division
- F-actin cortex re-organization induces oocyte contractions lasting several hours
- Cortex contractions impact organelle distribution and activity
- Cortex contractions impact mouse and human oocytes' developmental potential

Authors

Elvira Nikalayevich, Gaëlle Letort, Ghislain de Labbey, ..., Melina Schuh, Marie-Emilie Terret, Marie-Hélène Verlhac

Correspondence

marie-emilie.terret@college-de-france.fr (M.-E.T.), marie-helene.verlhac@college-de-france.fr (M.-H.V.)

In brief

Nikalayevich et al. show that mouse oocytes lacking an F-actin nucleator complex undergo cortex remodeling, triggering cortex contractions that perturb mouse and human oocyte cytoplasmic organization, affecting their quality. Contractions do not correlate with aneuploidy in mice or humans and represent a distinct type of anomaly, potentially associated with infertility.

Nikalayevich et al., 2024, Developmental Cell *59*, 1–12
April 8, 2024
https://doi.org/10.1016/j.devcel.2024.01.027

CellPress

Please cite this article in press as: Nikalayevich et al., Aberrant cortex contractions impact mammalian oocyte quality, Developmental Cell (2024), https://doi.org/10.1016/j.devcel.2024.01.027

Developmental Cell

CellPress
OPEN ACCESS

Short article

Aberrant cortex contractions impact mammalian oocyte quality

Elvira Nikalayevich,[1] Gaëlle Letort,[2] Ghislain de Labbey,[1] Elena Todisco,[3] Anastasia Shihabi,[1] Hervé Turlier,[1] Raphaël Voituriez,[4] Mohamed Yahiatene,[5] Xavier Pollet-Villard,[5] Metello Innocenti,[6] Melina Schuh,[3] Marie-Emilie Terret,[1,*] and Marie-Hélène Verlhac[1,7,*]

[1]Center for Interdisciplinary Research in Biology (CIRB), Collège de France, Université PSL, CNRS, INSERM, 75005 Paris, France
[2]Department of Developmental and Stem Cell Biology, Institut Pasteur, CNRS UMR 3738, Université Paris Cité, 25 rue du Dr. Roux, 75015 Paris, France
[3]Max Planck Institute for Multidisciplinary Sciences, Göttingen, Germany
[4]Laboratoire de Physique Théorique de la Matière Condensée (LPTMC), Laboratoire Jean Perrin, CNRS, Sorbonne Université, Paris, France
[5]Centre Assistance Médicale à la Procréation Nataliance, Groupe Mlab, Pôle Santé Oréliance, Saran, France
[6]Department of Biotechnology and Biosciences, University of Milano-Bicocca, Piazza della Scienza 2, 20126 Milan, Italy
[7]Lead contact
*Correspondence: marie-emilie.terret@college-de-france.fr (M.-E.T.), marie-helene.verlhac@college-de-france.fr (M.-H.V.)
https://doi.org/10.1016/j.devcel.2024.01.027

SUMMARY

The cortex controls cell shape. In mouse oocytes, the cortex thickens in an Arp2/3-complex-dependent manner, ensuring chromosome positioning and segregation. Surprisingly, we identify that mouse oocytes lacking the Arp2/3 complex undergo cortical actin remodeling upon division, followed by cortical contractions that are unprecedented in mammalian oocytes. Using genetics, imaging, and machine learning, we show that these contractions stir the cytoplasm, resulting in impaired organelle organization and activity. Oocyte capacity to avoid polyspermy is impacted, leading to a reduced female fertility. We could diminish contractions and rescue cytoplasmic anomalies. Similar contractions were observed in human oocytes collected as byproducts during IVF (*in vitro* fertilization) procedures. These contractions correlate with increased cytoplasmic motion, but not with defects in spindle assembly or aneuploidy in mice or humans. Our study highlights a multiscale effect connecting cortical F-actin, contractions, and cytoplasmic organization and affecting oocyte quality, with implications for female fertility.

INTRODUCTION

The acto-myosin cortex is crucial for cell-shape changes, migration, rounding, and accurate spindle positioning in mitosis.[1–3] It consists of the Arp2/3 (actin-related protein 2/3) complex and formins-nucleated actin filaments, crosslinkers, and myosin motors, whose ratios and interactions govern cortex properties.[4–9] Somatic cells' cortex thickness ranges between 50 and 400 nm, becoming thinner during division.[6,10,11] In oocytes from many species, the cortex is exceptionally thick, reaching several microns.[12–15] During mouse oocyte first meiotic division, cortex thickness increases due to nucleation of the Arp2/3 complex's branched actin filaments.[12] This actin layer chases myosin II, leading to a reduction in cortical tension, essential for spindle positioning.[12,16] Excessive actin nucleation results in too-soft oocytes with defects in spindle positioning and chromosome segregation.[12,16,17] To investigate the consequences of an absence of cortex thickening, we depleted the Arp2/3 complex through a conditional knockout of its core subunit, ArpC4.[18]

Surprisingly, *arpc4*$^{-/-}$ oocytes displayed prominent contractions, starting shortly after meiosis I resumption and continuing for several hours, subsiding just before anaphase I. In a variety of species,[15,19–23] the cortex of oocytes/eggs exhibits surface contraction waves (SCWs), manifesting as a single contraction band running through the cell surface, following a cell-cycle-dependent pattern.[15] Cortex contractions have been observed in mouse blastomeres,[24] yet they have never been reported in mammalian oocytes. The contractions from *arpc4*$^{-/-}$ oocytes depend on myosin II activity and on F-actin cortex re-organization. These cortex contractions were associated with increased cytoplasmic motion, affecting organelle size, positioning, activity, fertilization, and oocyte developmental potential. Consequently, the fertility of female mice carrying such oocytes was reduced. Unexpectedly, cortex contractions with a similar temporal pattern were observed in human oocytes. Although aneuploidy is the most common defect of human oocytes and its rate increases with maternal age,[25–28] such contractions did not correlate with spindle assembly defects or aneuploidy in mouse or human. Hence, they represent a different type of anomaly, which may be associated with infertility.

RESULTS

ArpC4 depletion prevents oocyte cortical thickening

To investigate additional functions of actin cortical thickening of mouse oocytes,[12] we employed a conditional knockout

Please cite this article in press as: Nikalayevich et al., Aberrant cortex contractions impact mammalian oocyte quality, Developmental Cell (2024), https://doi.org/10.1016/j.devcel.2024.01.027

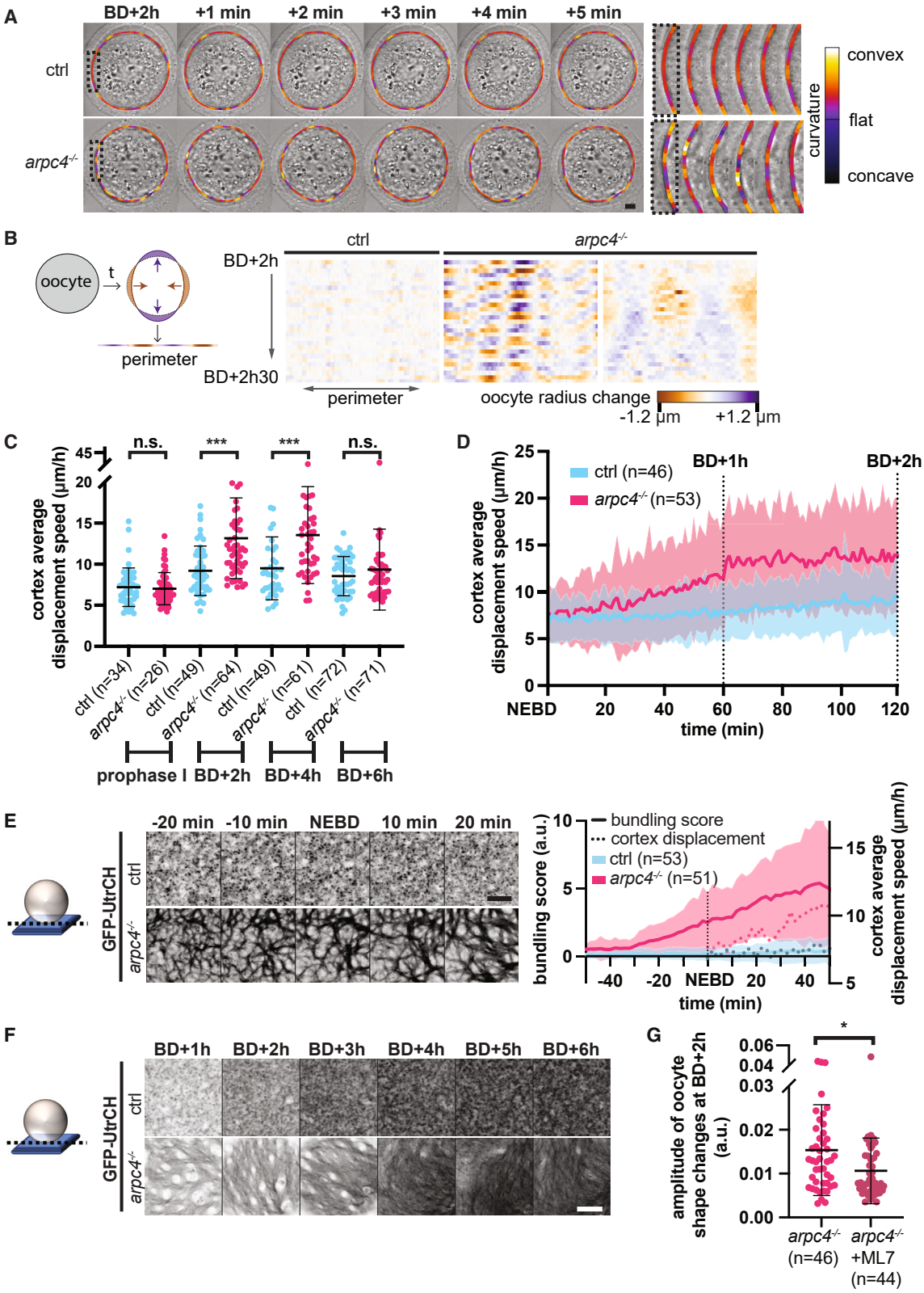

Figure 1. *Arpc4*$^{-/-}$ mouse oocytes display cortical contractions and prior F-actin cortex remodeling upon resumption of the first meiotic division

(A) Control (top) and *arpc4*$^{-/-}$ (bottom) oocytes time-lapse images in transillumination. The oocyte outlines are color-coded to reflect local curvatures. Right panels show time-lapse images of an enlarged portion of the oocyte, outlined with a dotted black box in the two left panels.

(legend continued on next page)

Please cite this article in press as: Nikalayevich et al., Aberrant cortex contractions impact mammalian oocyte quality, Developmental Cell (2024), https://doi.org/10.1016/j.devcel.2024.01.027

approach, using the ZP3-Cre line to ablate the expression of ArpC4, a core component of the Arp2/3 complex, in oocytes. This strategy enabled excision of exon 2 of ArpC4 (Figure S1A) exclusively in growing oocytes,[18,29] resulting in depletion of ArpC4 mRNA and protein (Figures S1B and S1C). ArpC4 being a core component of the Arp2/3 complex,[30] the depletion of ArpC4 led to a substantial reduction of other Arp2/3-complex subunits, including Arp3 and ArpC2 (Figure S1C), consistent with previous findings from mouse keratinocytes.[18] These results show that the entire Arp2/3 complex is absent in ArpC4 conditional knockout mouse oocytes (referred to as *arpc4*$^{-/-}$ oocytes).

Arp2/3-dependent cortical thickening is observed in meiosis I mouse oocytes and maximal around the first polar body extrusion[12,17] (PBE, an anaphase I marker). Consistently, *arpc4*$^{-/-}$ oocytes did not display cortical thickening, even at late stages of meiosis I (Figure S1D).

The depletion of the Arp2/3 complex impacted cortical thickening and not cytoplasmic F-actin (Figure S1E). This observation aligns with previous research indicating that the cytoplasmic F-actin mesh is nucleated by Formin 2 and Spire1/2, but not by the Arp2/3 complex.[12,17,31,32]

In conclusion, depletion of the Arp2/3 complex specifically prevented cortical thickening during mouse oocyte meiosis I.

Oocytes with no cortex thickening display contractions

To investigate the consequences of a lack of cortex thickening, we examined oocyte development through transmitted light time-lapse series. Control oocytes maintained a round shape, except during PBE. However, *arpc4*$^{-/-}$ oocytes exhibited prolonged and repeated contractions, characterized by shape changes (Figure 1A; Video S1).

To quantify these contractions, we measured oocyte radius change over time (Figure 1B). This allowed us to calculate the cortex average displacement speed (Figures 1C and 1D). Kymograph examples illustrating these changes in control and *arpc4*$^{-/-}$ oocytes are presented in Figure 1B. The contractions observed in *arpc4*$^{-/-}$ oocytes exhibited variability. They manifested as either rapid, small sequential bulges and retractions, lasting 2–3 min each (Figure 1B, middle kymograph; Video S1), or slower, large bulge-retraction sequences spanning tens of minutes (right kymograph; Video S1).

The average cortex displacement speed in controls was approximately 9 μm/h, reflecting the naturally slow changes in oocyte shape (Figure 1C). *arpc4*$^{-/-}$ oocytes did not contract in prophase I (Figure S1F; Video S1) but displayed an increase in cortical displacement speed from BD+2 h (breakdown, short for nuclear envelope breakdown) until BD+4 h (approximately 13 μm/h). Contractions decreased toward meiosis I end, being similar to controls (Figure 1C, BD+6 h).

Using higher temporal resolution movies, we observed a gradual increase in cortex average displacement speed in *arpc4*$^{-/-}$ oocytes, reaching a plateau around BD+1 h (Figure 1D).

These findings show that preventing cortical thickening induces hitherto unobserved cortical contractions during the first half of meiosis I.

F-actin remodeling precedes myosin-II-dependent cortex contractions

To gain further insights into the origin of contractions in *arpc4*$^{-/-}$ oocytes, we imaged the F-actin cortical structure. Controls displayed an isotropic actin network with patches of higher density and no observable structural changes around NEBD (nuclear envelope breakdown) (Figure 1E). In contrast, *arpc4*$^{-/-}$ oocytes exhibited F-actin bundles, increasing in thickness and eventually pulsating at tens of microns scale prior to meiosis resumption (Figure 1E; Video S2). We defined a "bundling score" by quantifying spatial correlations of nematic ordering of actin filaments (STAR Methods). Accordingly, the bundling rose 30 min before NEBD in mutants, while remaining low in controls (Figure 1E). Thick bundles disappeared in mutants 4 h after NEBD (Figure 1F), correlating with a reduction in contractions (Figure 1C). In summary, cortical remodeling observed in *arpc4*$^{-/-}$ oocytes preceded significant changes in oocyte shape (Figure 1E, compare the pink bold and dotted curves). This remodeling ceased during mid-meiosis I and was followed by a decrease in oocyte contractions (Figures 1F and 1C at BD+6 h). These observations indicate that cortical remodeling induces and regulates contractions in *arpc4*$^{-/-}$ oocytes.

Mechanical properties of actin networks depend on their architecture and motor activities.[33,34] We thus treated *arpc4*$^{-/-}$ oocytes with ML7, a myosin light chain kinase inhibitor required for promoting myosin II activity.[12,17,35] Addition of ML7 at BD+2 h, the contraction peak, reduced contractions (Figure 1G; Video S3). Hence, myosin II drives contractions in *arpc4*$^{-/-}$ oocytes.

arpc4$^{-/-}$ oocytes show cytoplasmic alterations

To further characterize *arpc4*$^{-/-}$ oocytes, we utilized our machine learning pipeline, Oocytor.[36] We subjected transmitted light movies of control and *arpc4*$^{-/-}$ developing oocytes to the Oocytor pipeline (STAR Methods). We then automatically

(B) Schematic and kymographs of oocyte radius changes over time. Horizontal axis corresponds to radius changes as measured at 100 points at the oocyte perimeter, with a time step of 1 min for 30 min (vertical axis). Radius shrinkage is in orange, radius growth in purple.
(C) Cortex average displacement speed in prophase I, then at 2, 4, and 6 h after NEBD. Data were gathered from 5, 3, 3, and 5 biological repeats for the respective time points.
(D) Cortex average displacement speed after NEBD (0 min) in control and *arpc4*$^{-/-}$ oocytes. Data were gathered from 3 biological repeats.
(E) Control (upper panel) and *arpc4*$^{-/-}$ oocytes (lower panel) time-lapse images of GFP-UtrCH (calponin homology domain of utrophin fused with GFP) labeled cortical F-actin around the time of NEBD. A cartoon (left) depicts how the cortex was imaged. The graph (right) displays the evolution of the bundling score (left y axis, solid lines) and of the cortex average displacement speed (right y axis, dotted lines) around the time of NEBD in control and *arpc4*$^{-/-}$ oocytes. Data were gathered from 6 biological repeats.
(F) Control (upper panel) and *arpc4*$^{-/-}$ oocytes (lower panel) show time-lapse images of GFP-UtrCH-labeled cortical F-actin from 1 to 6 h after NEBD.
(G) Amplitude of the oocyte shape changes at BD+2 h in *arpc4*$^{-/-}$ oocytes treated or not with ML7. Data were gathered from 3 biological repeats.
Scale bar is 10 μm (A) or 5 μm (E and F). In (C)–(E) and (G), means ±SD are shown, each dot is a value from 1 oocyte. n is the number of mouse oocytes. a.u., arbitrary units. n.s., not significant. *$p < 0.05$, ***$p < 0.001$.

Please cite this article in press as: Nikalayevich et al., Aberrant cortex contractions impact mammalian oocyte quality, Developmental Cell (2024), https://doi.org/10.1016/j.devcel.2024.01.027

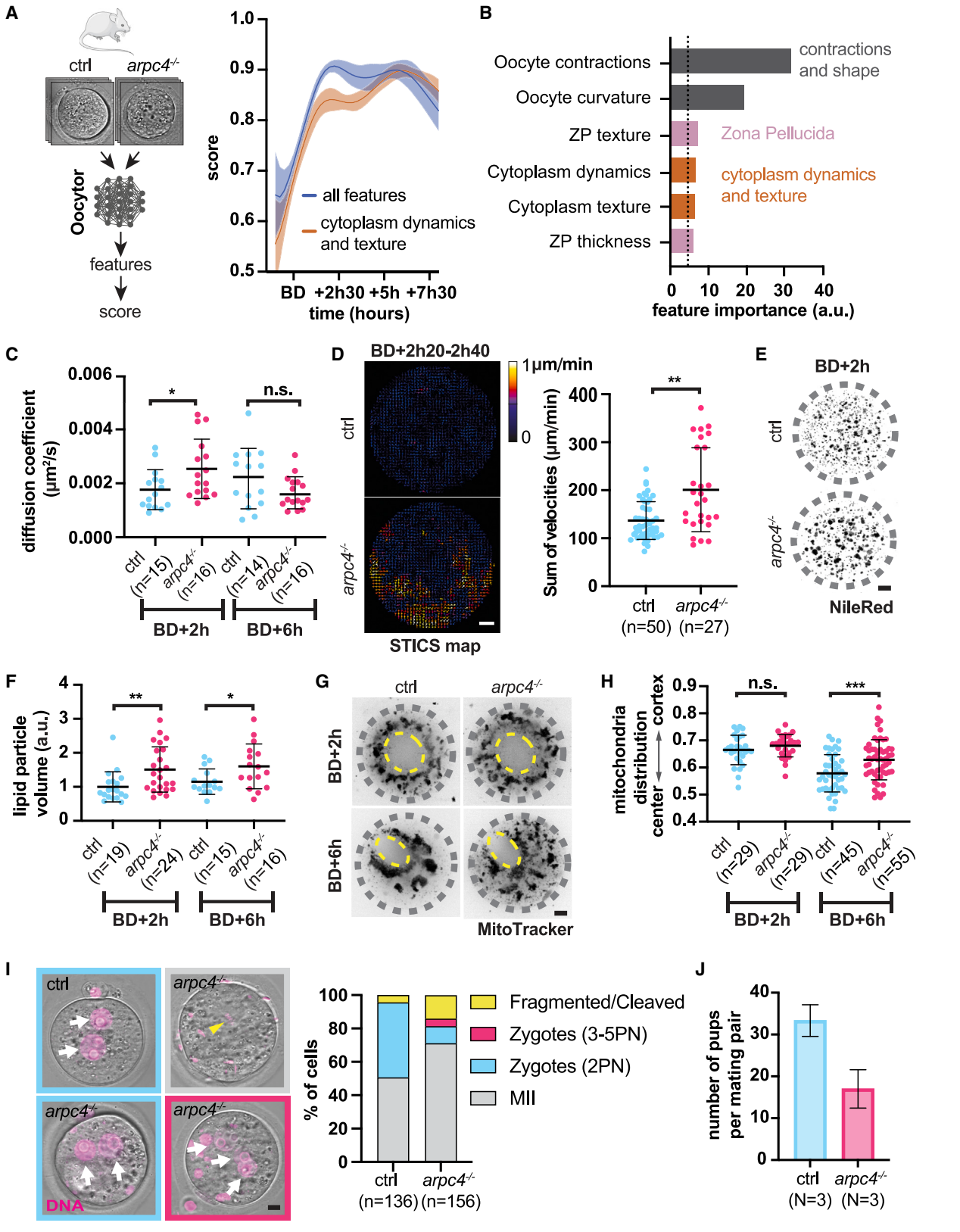

(legend on next page)

Please cite this article in press as: Nikalayevich et al., Aberrant cortex contractions impact mammalian oocyte quality, Developmental Cell (2024), https://doi.org/10.1016/j.devcel.2024.01.027

extracted static and dynamic morphological features from both oocyte types, which were used to train a classifier (Table S1A in https://zenodo.org/records/10567648). Discrimination between the two types was measured by a score: close to 1 indicated an effective discrimination, near 0.5 suggested random chance and limited discriminating capacity (Figure 2A). Discrimination was poor in prophase I, peaked at BD+2.5 h, and then declined (Figure 2A). Notably, cortex contractions were the most discriminant feature, followed by zona pellucida and cytoplasm (Figure 2B; Tables S1B and S1C in https://zenodo.org/records/10567648). When focusing solely on cytoplasmic features, discrimination was good from BD+2.5 h onward, with highest score during mid-meiosis I (Figure 2A).

Our approach revealed that *arpc4*$^{-/-}$ oocytes are indistinguishable from controls in prophase I. They display distinct characteristics after meiosis resumption, the most discriminant being contractions. Furthermore, besides cortex contractions, *arpc4*$^{-/-}$ oocytes exhibit phenotypes associated with cytoplasmic movement and appearance. These phenotypes are detected concurrently with contractions and become more prominent as meiosis I progresses.

arpc4$^{-/-}$ oocytes present organelle alterations and fertilization defects

To quantify cytoplasmic defects detected by Oocytor, we measured the motion of small lipid particles, as in Bennabi et al.,[17] Almonacid et al.,[37] and Colin et al.[38] In log-log scale, the slope of the mean squared displacement (MSD) curves was close to 1 in both controls and mutants, indicating that lipid particle movement was diffusive-like, as expected[37,38] (Figure S2A). Their diffusion coefficient was higher in *arpc4*$^{-/-}$ oocytes at BD+2 h, suggesting enhancement of their motion (Figure 2C). This increase in diffusion was concomitant with cortex contractions, with both phenomena diminishing after BD+6 h (Figure 2C). Contractions also impacted cytoplasmic flows, as evidenced by spatial temporal image correlation spectroscopy (STICS) maps performed at contraction peaks (Figure 2D and STAR Methods). Increased diffusion at short and long timescales (Figures 2C and 2D) correlated with larger clusters of lipid particles (Figure 2E). Their average volume was indeed significantly bigger in *arpc4*$^{-/-}$ oocytes (Figure 2F), but not in prophase I (Figure S2B). The augmented motion of lipid particles might raise encounter rates and thus the formation of larger clusters via coalescence, reminiscent of observations in oocyte nuclear condensates.[39]

We thus investigated whether other organelles were affected. Mitochondria accumulate around the oocyte spindle and into large cytoplasmic aggregates.[40,41] At BD+6 h, but not BD+2 h, mitochondria were less central in *arpc4*$^{-/-}$ oocytes (Figures 2G and 2H) and their membrane potential was lower (Figures S2C and S2D), suggesting that mitochondrial distribution and activity was impaired in mutants.

Cortical granules, organelles essential to prevent polyspermy, are synthesized in the cytoplasm and transported to the cortex during meiosis I.[42] Cortical granules in *arpc4*$^{-/-}$ oocytes formed patches and did not accumulate as a smooth cortical layer (Figure S2E), arguing that their transport and/or incorporation into the cortex was affected. Cortical granule defects can impact fertilization and the capacity to produce live progeny. *In vivo* fertilization experiments revealed that *arpc4*$^{-/-}$ oocytes produced few viable zygotes presenting 2 pronuclei (Figure 2I). Furthermore, *arpc4*$^{-/-}$ oocytes often failed to block polyspermy, remaining unfertilized with multiple sperm heads between zona pellucida and the membrane, or forming zygotes with 3 or more pronuclei (Figure 2I). This was consistent with cortical granule defects and zona pellucida alterations detected by Oocytor. The number of pups from mice carrying *arpc4*$^{-/-}$ oocytes was reduced roughly by half compared with controls (Figure 2J), attesting to a reduced fertility.

The energy generated by cortical contractions might be transmitted to the cytoplasm, leading to increased diffusion of lipid particles, increasing their volume, and compromising distribution and activity of many organelles, such as mitochondria and maybe cortical granules as well.

Reducing cortex contractions rescues cytoplasmic defects from *arpc4*$^{-/-}$ oocytes

To test the direct involvement of cortex contractions on cytoplasmic alterations, we inhibited them and checked for cytoplasmic phenotypes. ML7-treated oocytes displayed reduced

Figure 2. *arpc4*$^{-/-}$ mouse oocytes present cytoplasmic alterations and *in vivo* fertilization defects, and female mice are subfertile

(A) Left, Oocytor pipeline schematic used to identify morphological features different between control and *arpc4*$^{-/-}$ mouse oocytes. Right, Oocytor score evolution with meiosis progression and depending on the set of analyzed features. Means ± SEM are shown. Scores were calculated from 3 biological repeats.

(B) Feature importance ranking allowing Oocytor to discriminate between control and *arpc4*$^{-/-}$ oocytes at BD+2 h until BD+3 h. The dotted line represents the average of all the feature importance values.

(C) Diffusion coefficient of NileRed-stained particles at BD+2 h for 2 min in control and *arpc4*$^{-/-}$ oocytes. Data were gathered from 3 biological repeats.

(D) STICS maps (left) from transmitted light movies, with velocity vectors of cytoplasm measured from BD+2 h 20 min until BD+2 h 40 min in control (top) and *arpc4*$^{-/-}$ (bottom) oocytes. Summed velocities for each oocyte from these maps (right). Data were gathered from 7 biological repeats.

(E) Z projections of whole control (left) and *arpc4*$^{-/-}$ (right) oocytes stained with NileRed at BD+2 h. The gray dashed circle represents the oocyte outline.

(F) Size comparison of NileRed-stained particles in control and *arpc4*$^{-/-}$ oocytes cytoplasm at BD+2 h and BD+6 h. Data were gathered from 3 biological repeats.

(G) Single z slice of oocytes stained with MitoTracker in control (left) and *arpc4*$^{-/-}$ (right) oocytes at BD+2 h (top) and BD+6 h (bottom). The gray dashed circle represents the oocyte outline, and the yellow dashed ellipse represents the spindle.

(H) Distribution of MitoTracker-labeled large mitochondrial masses, measured on the center-cortex axis, averaged per oocyte, at BD+2 h and BD+6 h (4 and 5 biological repeats, respectively) in control and *arpc4*$^{-/-}$ oocytes.

(I) Mouse oocytes *in vivo* fertilization test. White arrows point to pronuclei, yellow arrowhead points to the metaphase II chromosomes. Hoechst stain is in magenta, transillumination images in gray. The graph (right) shows the frequency of unfertilized metaphase II oocytes (MII), normally fertilized zygotes (zygotes [2PN (pronuclei)]), polyspermic zygotes (zygotes [3PN–5PN]), and fragmented or cleaved zygotes (fragmented/cleaved). Data were gathered from 3 biological repeats.

(J) Mouse female fertility test (see STAR Methods). N is the number of mouse mating pairs.

Scale bar is 10 μm. In (C), (D), (F), (H), and (J) mean ± SD are shown, each dot is a value from 1 oocyte. n is the number of mouse zygotes and/or oocytes. n.s., not significant. *$p < 0.05$, **$p < 0.01$, ***$p < 0.001$.

Please cite this article in press as: Nikalayevich et al., Aberrant cortex contractions impact mammalian oocyte quality, Developmental Cell (2024), https://doi.org/10.1016/j.devcel.2024.01.027

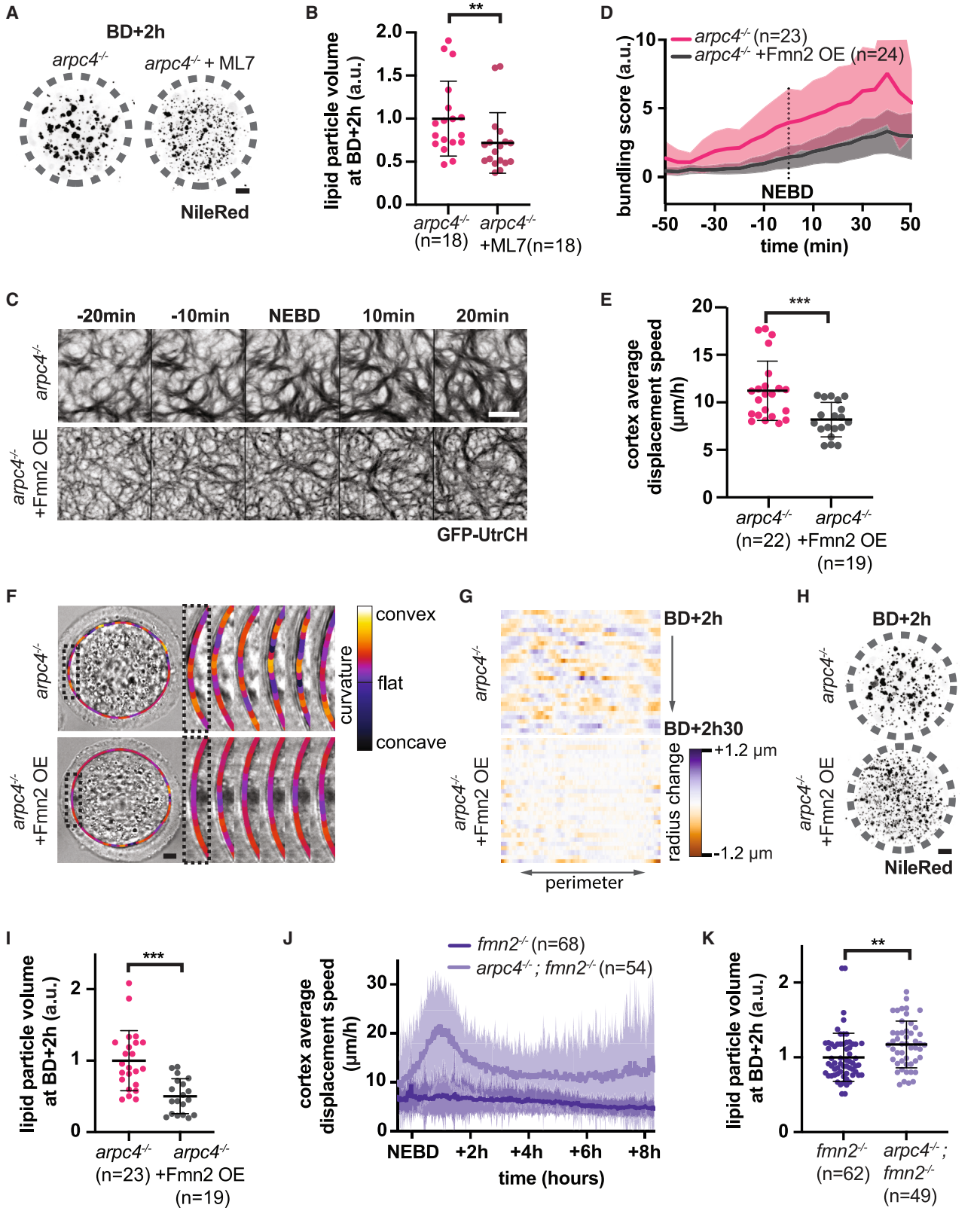

Figure 3. Rescue of *arpc4*$^{-/-}$ cytoplasmic alterations with myosin II inhibition or overexpression of Formin 2, but not with Formin 2 depletion

(A) Z projections of whole *arpc4*$^{-/-}$ oocytes, untreated (left) or treated (right) with ML7, stained with NileRed at BD+2 h. The gray dashed circle represents oocyte outline.

(legend continued on next page)

Please cite this article in press as: Nikalayevich et al., Aberrant cortex contractions impact mammalian oocyte quality, Developmental Cell (2024), https://doi.org/10.1016/j.devcel.2024.01.027

contractions (Figure 1G; Video S3) and smaller NileRed-positive particles (Figures 3A and 3B). Cortex contractions appeared and disappeared when another key nucleator, Formin 2, is degraded and resynthesized.[43] F-actin cortex re-organization into bundles was observed in *arpc4*$^{-/-}$ oocytes overexpressing Formin 2 (Video S2). However, the average bundling score was reduced compared with *arpc4*$^{-/-}$ oocytes (Figures 3C and 3D), along with cortex average displacement speed (Figure 3E), with cortical contraction reduction (Figures 3F and 3G; Video S3). Importantly, it also led to a notable decrease in lipid particle volume (Figures 3H and 3I).

The disappearance of Formin 2 might thus participate in cortex remodeling from *arpc4*$^{-/-}$ oocytes. Formin 2 resynthesis might also trigger disappearance of cortex contractions later on. To test this latter hypothesis, we checked whether contractions developed into double knockout oocytes (*arpc4*$^{-/-}$; *fmn2*$^{-/-}$). These double knockout oocytes displayed contractions with an appearance and a duration similar to those from *arpc4*$^{-/-}$ oocytes, whereas *fmn2*$^{-/-}$ oocytes did not contract (Figure 3J; Video S3). Although overexpressing Formin 2 diminished cortex contractions, the double knockout oocytes argue against a role for endogenous Formin 2 in the development of contractions. Interestingly, cortex contractions in *arpc4*$^{-/-}$; *fmn2*$^{-/-}$ oocytes correlated with a size increase in NileRed-positive particles compared with *fmn2*$^{-/-}$ oocytes (Figure 3K).

The different rescue experiments suggest that F-actin remodeling results in large-scale cortex contractions, leading to increased cytoplasmic diffusion, probably promoting lipid particle encounters and clustering, all being alleviated upon a reduction in contractions.

Low-quality human oocytes contract during the first meiotic division

We incidentally had access to a large collection of 244 movies of developing human oocytes coming from an IVF clinic. During fertility treatments, women are treated with hormones to stimulate development of several oocytes. Oocytes collected after such treatments are usually a mixture of metaphase-II-arrested ones, used for fertilization, as well as some still in prophase I. The latter ones are considered to be of low quality and are not used for IVF, as chances of successful embryonic development are low.[44–46] However, they are so far the only type of oocytes allowing the study of the first meiotic division from prophase I in human.

We analyzed transmitted light movies of these human oocytes using Oocytor (Figure 4A; Table S1D in https://zenodo.org/records/10567648). Some oocytes displayed temporary oscillatory changes in shape, reminiscent of cortex contractions detected in *arpc4*$^{-/-}$ mouse oocytes (Figure 4B; Video S4). Using Oocytor, we extracted the cortex average displacement rate from human movies. Similar to mouse *arpc4*$^{-/-}$ oocytes, human oocytes did not contract in prophase I (average cortex displacement 1.7 μm/h), but gradually increased contraction speed shortly after NEBD (up to 2.6 μm/h) and ceased contracting in the second half of metaphase I (1.5 μm/h) (Figure 4C). Human oocytes completed the first meiotic division and extruded a first polar body on average 14.9 h after NEBD, similar to previous work[47] (Figure S2F). Notably, *arpc4*$^{-/-}$ mouse oocytes were also able to extrude the first polar body at the same time and with similar efficiency as controls (Figure S2G). There was also no correlation (Spearman coefficient of 0.15) between the timing of PBE and the average cortex displacement speed in human oocytes (Figure S2H). We then assessed the effect of cortical contractions on mouse and human spindle assembly and chromosome segregation. In mouse oocytes, no differences in spindle morphology were detected between control and *arpc4*$^{-/-}$ (Figure S3A). Chromosome mis-segregation rates as well as the distance between the kinetochores of pairs of sisters were also not different (Figures S3B and S3C). Human oocytes coming from a different source of patients,[47] imaged live to follow chromosomes and microtubules,[47] were analyzed here differently than in Holubcová et al.[47] and did not display correlation between the presence of contractions and defects in spindle assembly, chromosome congression, or lagging chromosomes at anaphase (Figure S3D; Video S4).

These observations suggest that cortex contractions are a common feature of maturing human oocytes, not specific to

(B) Volume comparison of NileRed-stained lipid particles in *arpc4*$^{-/-}$ oocytes, untreated or treated with ML-7 at BD+2 h. Data were gathered from 3 biological repeats.
(C) Time-lapse images of cortical F-actin (labeled with GFP-UtrCH) in *arpc4*$^{-/-}$ oocytes (upper panel) and *arpc4*$^{-/-}$ oocytes overexpressing Formin 2 (lower panel).
(D) Evolution of the average bundling score around the time of NEBD (0 min) in *arpc4*$^{-/-}$ oocytes and *arpc4*$^{-/-}$ oocytes overexpressing Formin 2. Data were gathered from 3 biological repeats.
(E) Average cortex displacement speed in *arpc4*$^{-/-}$ and *arpc4*$^{-/-}$ overexpressing Formin 2 oocytes at BD+2 h. Data were gathered from 3 biological repeats.
(F) *arpc4*$^{-/-}$ (top) and *arpc4*$^{-/-}$ overexpressing Formin 2 (bottom) oocytes, transillumination images at BD+2 h. The oocyte outlines are color-coded to reflect local curvatures. Right panels show time-lapse images of an enlarged portion of the oocyte in a dotted black box on the two left panels, time points are every minute.
(G) Representative kymographs of radius changes over time in an *arpc4*$^{-/-}$ (top) and an *arpc4*$^{-/-}$ overexpressing Formin 2 oocyte (bottom). Horizontal axis corresponds to radius changes as measured at 100 points at the oocyte perimeter, with a time step of 1 min for 30 min (vertical axis). Radius shrinkage is in orange, radius growth in purple.
(H) Z projections of a whole *arpc4*$^{-/-}$ (left) and an *arpc4*$^{-/-}$ overexpressing Formin 2 (right) oocytes, stained with NileRed at BD+2 h. The gray dashed circle represents the oocyte outline.
(I) Volume comparison of NileRed-stained particles from *arpc4*$^{-/-}$ and *arpc4*$^{-/-}$ overexpressing Formin 2 oocytes. Data were gathered from 3 biological repeats.
(J) Cortex average displacement speed measured before NEBD in *fmn2*$^{-/-}$ and *arpc4*$^{-/-}$; *fmn2*$^{-/-}$ double knockout oocytes. Data were gathered from 3 biological repeats.
(K) Volume comparison of NileRed-stained particles from *fmn2*$^{-/-}$ and *arpc4*$^{-/-}$; *fmn2*$^{-/-}$ double knockout oocytes. Data were gathered from 4 biological repeats.
Scale bar is 10 μm in (A), (F), and (H) or 5 μm in (C). In (B), (E), (I), (J), and (K), mean ± SD are shown, each dot is a value from 1 oocyte. n is the number of mouse oocytes. a.u., arbitrary units. **$p < 0.01$, ***$p < 0.001$.

Please cite this article in press as: Nikalayevich et al., Aberrant cortex contractions impact mammalian oocyte quality, Developmental Cell (2024), https://doi.org/10.1016/j.devcel.2024.01.027

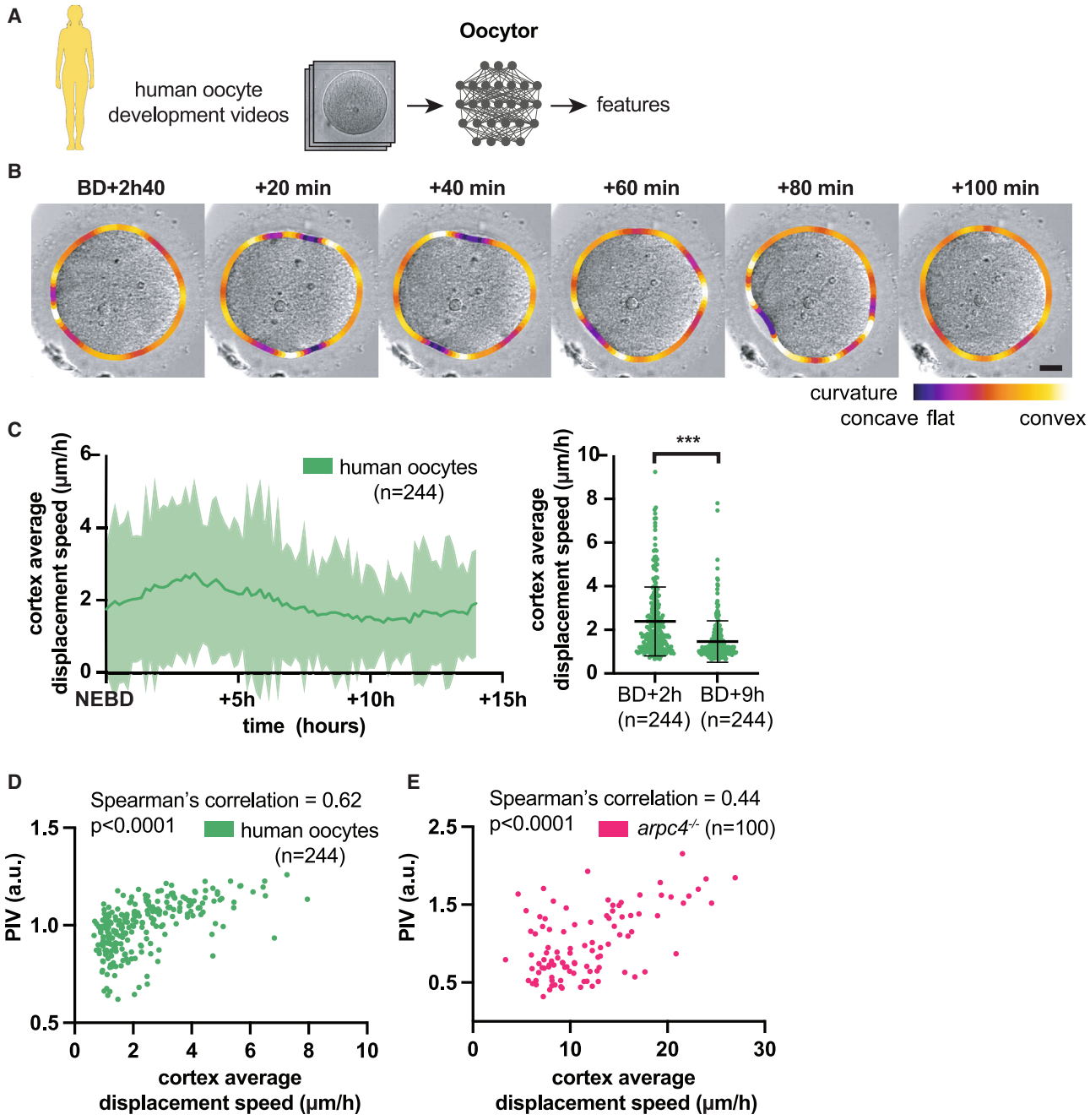

Figure 4. Human oocytes display cortical contractions similar to those present in *arpc4*$^{-/-}$ mouse oocytes

(A) Schematic of the Oocytor pipeline used to identify morphological features from time-lapse images of human oocytes observed during their first meiotic division.

(B) Human oocyte time-lapse images in transillumination. The oocyte outlines are color-coded to reflect local curvatures.

(C) Cortex average displacement speed of human oocytes during the first meiotic division from NEBD until BD+14 h (left). On the right, values from BD+2 h and BD+9 h from the same dataset are compared. Mean ± SD is shown.

(D) Cytoplasm stirring, measured with particle image velocity (PIV), plotted against the cortex average displacement speed between BD+2 h and BD+5 h in human oocytes.

(E) Cytoplasm stirring plotted against the cortex average displacement speed at BD+2 h in *arpc4*$^{-/-}$ mouse oocytes.

Scale bar is 20 µm. a.u., arbitrary units. In (D) and (E), each dot is a value from 1 oocyte. n is the number of human or mouse oocytes. ***p < 0.001.

Please cite this article in press as: Nikalayevich et al., Aberrant cortex contractions impact mammalian oocyte quality, Developmental Cell (2024), https://doi.org/10.1016/j.devcel.2024.01.027

the country, practice, or patients. They also suggest that contractions have no or very little influence on meiotic-cell-cycle length, spindle assembly, and chromosome segregation.

To further analyze the similarity between the two model systems (*arpc4*$^{-/-}$ oocytes versus human oocytes), we assessed cytoplasm dynamics by particle image velocity (PIV). We observed a significant positive correlation between cytoplasm dynamics and average cortex displacement speed, both in human and *arpc4*$^{-/-}$ mouse oocytes (Figures 4D and 4E), but not in control mouse oocytes (Figure S2I). Cortex contractions thus promote cytoplasmic motion, both in mouse and human. Altogether our findings argued that *arpc4*$^{-/-}$ oocytes were a good model to study a cytoplasmic defect linked to infertility in mice and unrelated to the most common one, i.e., aneuploidy.

DISCUSSION

Beyond controlling the geometry of division and chromosome segregation, we uncover a function for the F-actin cortical thickening observed during mouse meiosis I.[12,16,17] In the absence of Arp2/3, the oocyte cortex is massively restructured owing to the nucleation of long microfilaments, organized into bundles of increasing sizes. A similar process was observed in NIH-3T3 fibroblasts, where acute inhibition of the Arp2/3 complex with CK666 triggers a switch from an isotropic mesh to long, aligned actin bundles or stars.[48] However, such a phenomenon has never been observed in oocytes. In previous work, we treated oocytes with CK666 3 h after NEBD,[12] which is after cortex re-organization from *arpc4*$^{-/-}$ oocytes. Other studies in oocytes have not consistently given the timing of CK666 treatment relative to NEBD, and the effects of such treatment on cortex contractions in mouse, porcine, and goat oocytes were not reported.[49–51] These discrepancies may arise from differences between genetic depletion, spanning oocyte growth, and acute inhibition. For example, a reduction in cortex thickness in HeLa cells was achieved by genetic depletion of ArpC2 subunit of the Arp2/3 complex, but not with CK666 treatment.[6] The initiation of cortex restructuring in Arp2/3-deficient oocytes requires entry into meiosis I and coincides with the degradation of Formin 2.[43] Although we show that overexpression of Formin 2 in *arpc4*$^{-/-}$ oocytes can induce a partial rescue of cortex structure and contractions, the double knockout approach argues that endogenous Formin 2 is physiologically dispensable. Proper elucidation of the initiation of cortex restructuring in Arp2/3-deficient oocytes will need further investigation.

The emergence of contractions in the absence of branched actin in *arpc4*$^{-/-}$ oocytes is consistent with earlier studies.[33,34] Indeed, long bundles of microfilaments support contractility and create a more compliant network favoring large-scale contractions, while a branched network prevents mechanical deformations.[52] This uncovers another function of cortical thickening in mouse oocytes, namely to prevent excessive contractions causing cytoplasmic perturbations. SCWs in the oocytes of other species have been hypothesized to impact the cytoplasm. For example, in ascidian eggs an SCW is thought to drag the subcortical layer of the cytoplasm from the animal to the vegetal pole after fertilization.[53] In starfish oocytes, SCWs have been shown to create cytoplasmic flows, but these flows were deemed weak and not responsible for cytoplasmic particle mixing.[23] Our work demonstrates that contractions in mouse oocytes cause differences in cytoplasm dynamics and organelle placement. Cytoplasmic motion is extremely important, required for mixing of the cytoplasm in large cells and for the establishment of polarity.[54] In mouse oocytes, cytoplasmic stirring induced by local Arp2/3-dependent cortical polarization was observed in meiosis II and shown to maintain spindle anchoring to the cortex.[55] However, to our knowledge, large cortex contractions impacting organelle distribution have not been reported in mammalian dividing oocytes. Contracting mouse oocytes tend to form bigger clusters of lipid droplets, likely due to increased cytoplasm movements that promote their encountering. It has been reported that large lipid droplets act as mechanical stressors, inducing the indentation of the nucleus and causing DNA damage and cytoskeletal disruption.[56] During embryonic division, large heterogeneous clusters from *arpc4*$^{-/-}$ oocytes might also cause damage, be unevenly segregated between blastomeres, and lead to imbalanced material and energy stores.

In a portion of low-quality human oocytes, cortex contractions are naturally present from the start of the first meiotic division until several hours before anaphase I. This may indicate that the human oocyte cortex has different properties than wild-type mouse cortices and might be more prone to forming contractile structures. Consistent with this, RNA sequencing (RNA-seq) and ribosome sequencing (Riboseq) data from prophase I human oocytes[57] show that the levels of subunits of the Arp2/3 complex are extremely variable. In particular, ArpC4 and ArpC5 seem to be expressed at very low levels in prophase I. Future work could test whether such observations explain the cortex contraction-prone nature of these cells. Contracting Arp2/3-complex-deficient mouse oocytes have a lower chance of developmental success. The appearance of contractions in developing human oocytes may represent a distinct factor of cytoplasmic infertility different from aneuploidy. Previous works show the correlation of oocyte developmental potential with organelle size, quantity, and distribution, as reviewed for mitochondria, lipid droplets, and cortical granules.[58] Future experiments are required to determine whether contracting human oocytes might display an altered organelle status associated with a lower chance of successful development. These oocytes are generally not used for medical applications; however, some patients may not have better options. In this case, the presence or absence of cortex contractions may help identify oocytes with higher chances of a good outcome.

Limitations of the study

Although our study has demonstrated a fundamental role for the Arp2/3 complex in preventing F-actin cortex remodeling and cortical contractions in mouse oocytes, future studies will address the potential limitations of our work. For example, although we examined the capacity of another nucleator, Formin 2, to rescue the lack of an Arp2/3 complex, further investigation is required to determine which endogenous nucleator prevents the appearance of cortex contractions or why cortex remodeling and contractions only appear when meiosis resumes. Additionally, our study does not provide a correlation between ArpC4 levels and the presence of contractions in human oocytes. This aspect needs further investigation. Finally, investigations of data from patients who donated human oocytes will offer the chance to further correlate our findings

with a diverse array of conditions characterized by the donor status, such as age, known to be a key factor influencing oocyte quality.

STAR★METHODS

Detailed methods are provided in the online version of this paper and include the following:

- KEY RESOURCES TABLE
- RESOURCE AVAILABILITY
  - Lead contact
  - Materials availability
  - Data and code availability
- EXPERIMENTAL MODEL AND STUDY PARTICIPANT DETAILS
  - Animal model
  - Human oocytes sources
- METHOD DETAILS
  - Mouse oocyte collection and culture
  - Human prophase I oocytes collection, processing and culture
  - Human prophase I oocyte image acquisition
  - RT-PCR
  - Immunoblotting and antibodies
  - Constructs, *in vitro* transcription of cRNA and microinjection
  - Drug treatments
  - Live imaging
- QUANTIFICATION AND STATISTICAL ANALYSIS
  - Spindle morphology measurements
  - Cortical thickness and F-actin in the cytoplasm
  - Cytoplasmic activity measurements
  - STICS measurements
  - Lipid particle volume
  - Mitochondria distribution
  - Mitochondria activity assay
  - Chromosome counting and measure of kinetochore distance between sister pairs in intact oocytes on monastrol spreads
  - Fertilization assay
  - Fertility assay
  - Machine learning approach for mouse oocyte morphological characterization
  - Machine learning approach for human oocyte movie analysis
  - PIV from trans images
  - Curvature measurements
  - Radii change kymographs and cortex displacement speed measurements
  - Amplitude of oocyte shape change
  - Bundling score
  - Statistical analysis
  - Image treatment and figure preparation

SUPPLEMENTAL INFORMATION

Supplemental information can be found online at https://doi.org/10.1016/j.devcel.2024.01.027.

ACKNOWLEDGMENTS

We thank all members of the Verlhac-Terret laboratory for discussions, Christelle Da Silva and Flora Crozet for preliminary experiments, the CIRB animal and Orion facilities, and especially Philippe Mailly for help with the analysis of lipid particle movements and volume quantifications. The Verlhac-Terret laboratory is supported by CNRS, INSERM, Collège de France, and the Bettencourt Schueller Foundation. This work received support under the program « Investissements d'Avenir », launched by the French Government and implemented by the ANR, with the references: ANR-10-LABX-54 MEMO LIFE and ANR-11-IDEX-0001-02 PSL* Research University, and through grants from the Fondation pour la Recherche Médicale (FRM label DEQ201903007796 to M.-H.V.), the ANR (ANR-18-CE13 and ANR-22-CE13 to M.-H.V.), and the InCa (PREVBIO 2021-161 to M.-H.V.). H.T. is supported by the CNRS and the Collège de France and has received funding from the European Research Council (ERC) under the Horizon 2020 research and innovation program of the European Union (grant agreement no. 949267). E.T. is supported by the Deutsche Forschungsgemeinschaft (DFG, German Research Foundation, 449750155 - RTG 2756, Project B5).

AUTHOR CONTRIBUTIONS

M.-H.V. conceived the project, which was supervised by M.-H.V. and M.-E.T. E.N. designed, performed, and analyzed all experiments on mouse oocytes. G.L. performed all analysis using the Oocytor pipeline. G.d.L. and H.T. designed the plugin to measure the F-actin cortex bundle score. R.V. provided insights on biophysics aspects of the work. M.Y. and X.P.-V. provided the human oocyte transmitted light videos. A.S. did the STICS maps analysis. M.I. provided the *arpc4* flox mouse line. E.T. and M.S. analyzed fluorescent movies coming from dividing human oocytes. E.N., R.V., and M.-H.V. wrote the manuscript, which was seen and corrected by all authors.

DECLARATION OF INTERESTS

The authors declare no competing interests.

Received: September 26, 2023
Revised: December 18, 2023
Accepted: January 26, 2024
Published: February 21, 2024

REFERENCES

1. Levayer, R., and Lecuit, T. (2013). Oscillation and polarity of E-cadherin asymmetries control actomyosin flow patterns during morphogenesis. Dev. Cell *26*, 162–175.
2. Chugh, P., and Paluch, E.K. (2018). The actin cortex at a glance. J. Cell Sci. *131*, jcs186254.
3. Taubenberger, A.V., Baum, B., and Matthews, H.K. (2020). The Mechanics of Mitotic Cell Rounding. Front. Cell Dev. Biol. *8*, 687.
4. Svitkina, T.M. (2020). Actin Cell Cortex: Structure and Molecular Organization. Trends Cell Biol. *30*, 556–565.
5. Levayer, R., and Lecuit, T. (2012). Biomechanical regulation of contractility: spatial control and dynamics. Trends Cell Biol. *22*, 61–81.
6. Chugh, P., Clark, A.G., Smith, M.B., Cassani, D.A.D., Dierkes, K., Ragab, A., Roux, P.P., Charras, G., Salbreux, G., and Paluch, E.K. (2017). Actin cortex architecture regulates cell surface tension. Nat. Cell Biol. *19*, 689–697.
7. Taneja, N., Bersi, M.R., Baillargeon, S.M., Fenix, A.M., Cooper, J.A., Ohi, R., Gama, V., Merryman, W.D., and Burnette, D.T. (2020). Precise Tuning of Cortical Contractility Regulates Cell Shape during Cytokinesis. Cell Rep. *31*, 107477.
8. Turlier, H., Audoly, B., Prost, J., and Joanny, J.-F. (2014). Furrow constriction in animal cell cytokinesis. Biophys. J. *106*, 114–123.
9. Sedzinski, J., Biro, M., Oswald, A., Tinevez, J.-Y., Salbreux, G., and Paluch, E. (2011). Polar actomyosin contractility destabilizes the position of the cytokinetic furrow. Nature *476*, 462–466.

10. Clausen, M.P., Colin-York, H., Schneider, F., Eggeling, C., and Fritzsche, M. (2017). Dissecting the actin cortex density and membrane-cortex distance in living cells by super-resolution microscopy. J. Phys. D Appl. Phys. *50*, 064002.

11. Clark, A.G., Dierkes, K., and Paluch, E.K. (2013). Monitoring Actin Cortex Thickness in Live Cells. Biophys. J. *105*, 570–580.

12. Chaigne, A., Campillo, C., Gov, N.S., Voituriez, R., Azoury, J., Umaña-Diaz, C., Almonacid, M., Queguiner, I., Nassoy, P., Sykes, C., et al. (2013). A soft cortex is essential for asymmetric spindle positioning in mouse oocytes. Nat. Cell Biol. *15*, 958–966.

13. Heil-Chapdelaine, R.A., and Otto, J.J. (1996). Characterization of Changes in F-actin during Maturation of Starfish Oocytes. Dev. Biol. *177*, 204–216.

14. Prodon, F., Chenevert, J., and Sardet, C. (2006). Establishment of animal–vegetal polarity during maturation in ascidian oocytes. Dev. Biol. *290*, 297–311.

15. Bischof, J., Brand, C.A., Somogyi, K., Májer, I., Thome, S., Mori, M., Schwarz, U.S., and Lénárt, P. (2017). A cdk1 gradient guides surface contraction waves in oocytes. Nat. Commun. *8*, 849.

16. Chaigne, A., Campillo, C., Gov, N.S., Voituriez, R., Sykes, C., Verlhac, M.H., and Terret, M.E. (2015). A narrow window of cortical tension guides asymmetric spindle positioning in the mouse oocyte. Nat. Commun. *6*, 6027.

17. Bennabi, I., Crozet, F., Nikalayevich, E., Chaigne, A., Letort, G., Manil-Ségalen, M., Campillo, C., Cadart, C., Othmani, A., Attia, R., et al. (2020). Artificially decreasing cortical tension generates aneuploidy in mouse oocytes. Nat. Commun. *11*, 1649.

18. van der Kammen, R., Song, J.-Y., de Rink, I., Janssen, H., Madonna, S., Scarponi, C., Albanesi, C., Brugman, W., and Innocenti, M. (2017). Knockout of the Arp2/3 complex in epidermis causes a psoriasis-like disease hallmarked by hyperactivation of transcription factor Nrf2. Development *144*, 4588–4603.

19. Yoneda, M., Kobayakawa, Y., Kubota, H.Y., and Sakai, M. (1982). Surface contraction waves in amphibian eggs. J. Cell Sci. *54*, 35–46.

20. Amiel, A., and Houliston, E. (2009). Three distinct RNA localization mechanisms contribute to oocyte polarity establishment in the cnidarian Clytia hemisphaerica. Dev. Biol. *327*, 191–203.

21. Prodon, F., Sardet, C., and Nishida, H. (2008). Cortical and cytoplasmic flows driven by actin microfilaments polarize the cortical ER-mRNA domain along the a–v axis in ascidian oocytes. Dev. Biol. *313*, 682–699.

22. Hara, K. (1971). Cinematographic observation of "surface contraction waves" (SCW) during the early cleavage of axolotl eggs. Wilhelm Roux. Arch. Entwickl. Mech. Org. *167*, 183–186.

23. Klughammer, N., Bischof, J., Schnellbächer, N.D., Callegari, A., Lénárt, P., and Schwarz, U.S. (2018). Cytoplasmic flows in starfish oocytes are fully determined by cortical contractions. PLoS Comput. Biol. *14*, e1006588.

24. Özgüç, Ö., de Plater, L., Kapoor, V., Tortorelli, A.F., Clark, A.G., and Maître, J.-L. (2022). Cortical softening elicits zygotic contractility during mouse preimplantation development. PLoS Biol. *20*, e3001593.

25. Nagaoka, S.I., Hassold, T.J., and Hunt, P.A. (2012). Human aneuploidy: mechanisms and new insights into an age-old problem. Nat. Rev. Genet. *13*, 493–504.

26. Hassold, T., and Hunt, P. (2001). To err (meiotically) is human: the genesis of human aneuploidy. Nat. Rev. Genet. *2*, 280–291.

27. Hassold, T., Hall, H., and Hunt, P. (2007). The origin of human aneuploidy: where we have been, where we are going. Hum. Mol. Genet. *16*, R203–R208.

28. Gruhn, J.R., Zielinska, A.P., Shukla, V., Blanshard, R., Capalbo, A., Cimadomo, D., Nikiforov, D., Chan, A.C.-H., Newnham, L.J., Vogel, I., et al. (2019). Chromosome errors in human eggs shape natural fertility over reproductive life span. Science *365*, 1466–1469.

29. Lewandoski, M., Wassarman, K.M., and Martin, G.R. (1997). Zp3-cre, a transgenic mouse line for the activation or inactivation of loxP-flanked target genes specifically in the female germ line. Curr. Biol. *7*, 148–151.

30. Pizarro-Cerdá, J., Chorev, D.S., Geiger, B., and Cossart, P. (2017). The Diverse Family of Arp2/3 Complexes. Trends Cell Biol. *27*, 93–100.

31. Azoury, J., Lee, K.W., Georget, V., Rassinier, P., Leader, B., and Verlhac, M.-H. (2008). Spindle positioning in mouse oocytes relies on a dynamic meshwork of actin filaments. Curr. Biol. *18*, 1514–1519.

32. Pfender, S., Kuznetsov, V., Pleiser, S., Kerkhoff, E., and Schuh, M. (2011). Spire-type actin nucleators cooperate with Formin-2 to drive asymmetric oocyte division. Curr. Biol. *21*, 955–960.

33. Alvarado, J., Sheinman, M., Sharma, A., MacKintosh, F.C., and Koenderink, G.H. (2017). Force percolation of contractile active gels. Soft Matter *13*, 5624–5644.

34. Ennomani, H., Letort, G., Guérin, C., Martiel, J.-L., Cao, W., Nédélec, F., De La Cruz, E.M., Théry, M., and Blanchoin, L. (2016). Architecture and Connectivity Govern Actin Network Contractility. Curr. Biol. *26*, 616–626.

35. Schuh, M., and Ellenberg, J. (2008). A New Model for Asymmetric Spindle Positioning in Mouse Oocytes. Curr. Biol. *18*, 1986–1992.

36. Letort, G., Eichmuller, A., Da Silva, C., Nikalayevich, E., Crozet, F., Salle, J., Minc, N., Labrune, E., Wolf, J.-P., Terret, M.-E., and Verlhac, M.-H. (2022). An interpretable and versatile machine learning approach for oocyte phenotyping. J. Cell Sci. *135*, jcs260281.

37. Almonacid, M., Ahmed, W.W., Bussonnier, M., Mailly, P., Betz, T., Voituriez, R., Gov, N.S., and Verlhac, M.-H. (2015). Active diffusion positions the nucleus in mouse oocytes. Nat. Cell Biol. *17*, 470–479.

38. Colin, A., Letort, G., Razin, N., Almonacid, M., Ahmed, W., Betz, T., Terret, M.-E., Gov, N.S., Voituriez, R., Gueroui, Z., and Verlhac, M.-H. (2020). Active diffusion in oocytes nonspecifically centers large objects during prophase I and meiosis I. J. Cell Biol. *219*, e201908195.

39. Al Jord, A., Letort, G., Chanet, S., Tsai, F.-C., Antoniewski, C., Eichmuller, A., Da Silva, C., Huynh, J.-R., Gov, N.S., Voituriez, R., et al. (2022). Cytoplasmic forces functionally reorganize nuclear condensates in oocytes. Nat. Commun. *13*, 5070.

40. Cheng, S., Altmeppen, G., So, C., Welp, L.M., Penir, S., Ruhwedel, T., Menelaou, K., Harasimov, K., Stützer, A., Blayney, M., et al. (2022). Mammalian oocytes store mRNAs in a mitochondria-associated membraneless compartment. Science *378*, eabq4835.

41. Dalton, C.M., and Carroll, J. (2013). Biased inheritance of mitochondria during asymmetric cell division in the mouse oocyte. J. Cell Sci. *126*, 2955–2964.

42. Cheeseman, L.P., Boulanger, J., Bond, L.M., and Schuh, M. (2016). Two pathways regulate cortical granule translocation to prevent polyspermy in mouse oocytes. Nat. Commun. *7*, 13726.

43. Azoury, J., Lee, K.W., Georget, V., Hikal, P., and Verlhac, M.-H. (2011). Symmetry breaking in mouse oocytes requires transient F-actin meshwork destabilization. Development *138*, 2903–2908.

44. Avci, B., Kasapoglu, I., Cakir, C., Ozbay, A., Ata, B., and Uncu, G. (2022). Fertilisation and early embryonic development of immature and rescue in vitro-matured sibling oocytes. Hum. Fertil. (Camb) *25*, 107–116.

45. Lacham-Kaplan, O., and Trounson, A. (2008). Reduced developmental competence of immature, in-vitro matured and postovulatory aged mouse oocytes following IVF and ICSI. Reprod. Biol. Endocrinol. *6*, 58.

46. Margalit, T., Ben-Haroush, A., Garor, R., Kotler, N., Shefer, D., Krasilnikov, N., Tzabari, M., Oron, G., Shufaro, Y., and Sapir, O. (2019). Morphokinetic characteristics of embryos derived from in-vitro-matured oocytes and their in-vivo-matured siblings after ovarian stimulation. Reprod. Biomed. Online *38*, 7–11.

47. Holubcová, Z., Blayney, M., Elder, K., and Schuh, M. (2015). Human oocytes. Error-prone chromosome-mediated spindle assembly favors chromosome segregation defects in human oocytes. Science *348*, 1143–1147.

48. Eghiaian, F., Rigato, A., and Scheuring, S. (2015). Structural, Mechanical, and Dynamical Variability of the Actin Cortex in Living Cells. Biophys. J. *108*, 1330–1340.

49. Sun, S.-C., Wang, Z.-B., Xu, Y.-N., Lee, S.-E., Cui, X.-S., and Kim, N.-H. (2011). Arp2/3 complex regulates asymmetric division and cytokinesis in mouse oocytes. PloS One *6*, e18392.

50. Wang, F., An, G.-Y., Zhang, Y., Liu, H.-L., Cui, X.-S., Kim, N.-H., and Sun, S.-C. (2014). Arp2/3 complex inhibition prevents meiotic maturation in porcine oocytes. PloS One *9*, e87700.

51. Pan, M.-H., Xu, R., Zhang, Y., Yin, L., Li, R., Wen, D., Lu, S., Gao, Y., Zhao, X., Wei, Q., et al. (2023). The Impact of Arp2/3 Complex Inhibition on Cytoskeleton Dynamics and Mitochondrial Function during Goat Oocyte Meiosis. Animals (Basel) *13*, 263.

52. Muresan, C.G., Sun, Z.G., Yadav, V., Tabatabai, A.P., Lanier, L., Kim, J.H., Kim, T., and Murrell, M.P. (2022). F-actin architecture determines constraints on myosin thick filament motion. Nat. Commun. *13*, 7008.

53. Sawada, T.-O., and Osanai, K. (1981). The cortical contraction related to the ooplasmic segregation inCiona intestinalis eggs. Wilhelm Rouxs Arch. Dev. Biol. *190*, 208–214.

54. Lu, W., and Gelfand, V.I. (2023). Go with the flow – bulk transport by molecular motors. J. Cell Sci. *136*, jcs260300.

55. Yi, K., Unruh, J.R., Deng, M., Slaughter, B.D., Rubinstein, B., and Li, R. (2011). Dynamic maintenance of asymmetric meiotic spindle position through Arp2/3 complex-driven cytoplasmic streaming in mouse oocytes. Nat. Cell Biol. *13*, 1252–1258.

56. Loneker, A.E., Alisafaei, F., Kant, A., Li, D., Janmey, P.A., Shenoy, V.B., and Wells, R.G. (2023). Lipid droplets are intracellular mechanical stressors that impair hepatocyte function. Proc. Natl. Acad. Sci. USA *120*, e2216811120.

57. Hu, W., Zeng, H., Shi, Y., Zhou, C., Huang, J., Jia, L., Xu, S., Feng, X., Zeng, Y., Xiong, T., et al. (2022). Single-cell transcriptome and translatome dual-omics reveals potential mechanisms of human oocyte maturation. Nat. Commun. *13*, 5114.

58. Reader, K.L., Stanton, J.-A.L., and Juengel, J.L. (2017). The Role of Oocyte Organelles in Determining Developmental Competence. Biology *6*, 35.

59. Leader, B., Lim, H., Carabatsos, M.J., Harrington, A., Ecsedy, J., Pellman, D., Maas, R., and Leder, P. (2002). Formin-2, polyploidy, hypofertility and positioning of the meiotic spindle in mouse oocytes. Nat. Cell Biol. *4*, 921–928.

60. Tsurumi, C., Hoffmann, S., Geley, S., Graeser, R., and Polanski, Z. (2004). The spindle assembly checkpoint is not essential for CSF arrest of mouse oocytes. J. Cell Biol. *167*, 1037–1050.

61. Wu, T., Lane, S.I.R., Morgan, S.L., and Jones, K.T. (2018). Spindle tubulin and MTOC asymmetries may explain meiotic drive in oocytes. Nat. Commun. *9*, 2952.

62. Schindelin, J., Arganda-Carreras, I., Frise, E., Kaynig, V., Longair, M., Pietzsch, T., Preibisch, S., Rueden, C., Saalfeld, S., Schmid, B., et al. (2012). Fiji: an open-source platform for biological-image analysis. Nat. Methods *9*, 676–682.

63. Thévenaz, P., Ruttimann, U.E., and Unser, M. (1998). A pyramid approach to subpixel registration based on intensity. IEEE Trans. Image Process. *7*, 27–41.

64. Tinevez, J.-Y., Perry, N., Schindelin, J., Hoopes, G.M., Reynolds, G.D., Laplantine, E., Bednarek, S.Y., Shorte, S.L., and Eliceiri, K.W. (2017). TrackMate: An open and extensible platform for single-particle tracking. Methods *115*, 80–90.

65. Lowe, D.G. (2004). Distinctive Image Features from Scale-Invariant Keypoints. Int. J. Comput. Vis. *60*, 91–110.

66. Tarantino, N., Tinevez, J.-Y., Crowell, E.F., Boisson, B., Henriques, R., Mhlanga, M., Agou, F., Israël, A., and Laplantine, E. (2014). TNF and IL-1 exhibit distinct ubiquitin requirements for inducing NEMO-IKK supramolecular structures. J. Cell Biol. *204*, 231–245.

67. Verlhac, M.H., Lefebvre, C., Guillaud, P., Rassinier, P., and Maro, B. (2000). Asymmetric division in mouse oocytes: with or without Mos. Curr. Biol. *10*, 1303–1306.

68. Terret, M.E., Lefebvre, C., Djiane, A., Rassinier, P., Moreau, J., Maro, B., and Verlhac, M.-H. (2003). DOC1R: a MAP kinase substrate that control microtubule organization of metaphase II mouse oocytes. Development *130*, 5169–5177.

69. Yi, K., Rubinstein, B., Unruh, J.R., Guo, F., Slaughter, B.D., and Li, R. (2013). Sequential actin-based pushing forces drive meiosis I chromosome migration and symmetry breaking in oocytes. J. Cell Biol. *200*, 567–576.

70. Hebert, B., Costantino, S., and Wiseman, P.W. (2005). Spatiotemporal image correlation spectroscopy (STICS) theory, verification, and application to protein velocity mapping in living CHO cells. Biophys. J. *88*, 3601–3614.

71. Crozet, F., Letort, G., Bulteau, R., Da Silva, C., Eichmuller, A., Tortorelli, A.F., Blévinal, J., Belle, M., Dumont, J., Piolot, T., et al. (2023). Filopodia-like protrusions of adjacent somatic cells shape the developmental potential of oocytes. Life Sci. Alliance *6*, e202301963.

72. Tseng, Q., Duchemin-Pelletier, E., Deshiere, A., Balland, M., Guillou, H., Filhol, O., and Théry, M. (2012). Spatial organization of the extracellular matrix regulates cell–cell junction positioning. Proc. Natl. Acad. Sci. *109*, 1506–1511.

73. van der Walt, S., Schönberger, J.L., Nunez-Iglesias, J., Boulogne, F., Warner, J.D., Yager, N., Gouillart, E., and Yu, T.; scikit-image contributors (2014). scikit-image: image processing in Python. PeerJ *2*, e453.

74. Virtanen, P., Gommers, R., Oliphant, T.E., Haberland, M., Reddy, T., Cournapeau, D., Burovski, E., Peterson, P., Weckesser, W., Bright, J., et al. (2020). SciPy 1.0: fundamental algorithms for scientific computing in Python. Nat. Methods *17*, 261–272.

Please cite this article in press as: Nikalayevich et al., Aberrant cortex contractions impact mammalian oocyte quality, Developmental Cell (2024), https://doi.org/10.1016/j.devcel.2024.01.027

STAR★METHODS

KEY RESOURCES TABLE

REAGENT or RESOURCE	SOURCE	IDENTIFIER
Antibodies		
Goat Anti-ARPC4 Antibody	Everest Biotech	Cat#EB08249; RRID:AB_2274344
ARPC2 polyclonal antibody	ProteinTech	Cat #15058-1-AP; RRID:AB_2059787
Anti-Arp3 antibody [FMS338]	Abcam	Cat #ab49671; RRID:AB_2257830
ERK 1 Antibody (K-23)	Santa Cruz Biotechnology	Cat #sc-94; RRID:AB_2140110
Mouse IgG HRP Linked Whole Ab	Cytiva	Cat# NA931; RRID:AB_772210
Rabbit IgG HRP Linked Whole Ab	Cytiva	Cat# GENA934; RRID:AB_2722659
Chemicals, peptides, and recombinant proteins		
ML7	Merck	Cat#I2764; CAS: 110448-33-4
Monastrol	Sigma	Cat#M8515; CAS: 254753-54-3
Sir-Tubulin	Spirochrome	Cat#SC006
Milrinone	Merck	Cat#M4659; CAS: 78415-72-2
MitoTracker™ Red CMXRos	Thermofisher	Cat#M7512; CAS: 167095-09-2
TMRM dye	ThermoFisher	Cat#T668, CAS: 115532-50-8
Nile red	Sigma	Cat#N3013, CAS: 7385-67-3
Pregnant mare serum gonadotropin	Centravet	#PMS005
Human chorionic gonadotropin	Centravet	#CHO0003
Hoechst 33342	Thermofisher	#H3570
Critical commercial assays		
SignalBoost™ Immunoreaction Enhancer Kit	Millipore	Cat#407207-1KIT
Thermo Scientific™ SuperSignal™ West Femto Maximum Sensitivity Substrate	Fisher Scientific	Cat#11859290
RNAqueous™-Micro Total RNA Isolation Kit	ThermoFisher	Cat#AM1931
iScript™ Reverse Transcription Supermix	Bio-Rad	Cat#1708841
Deposited data		
Table S1. Values of features automatically extracted with Oocytor from transmitted light videos from mouse and human oocytes	This paper	https://zenodo.org/records/10567648 https://doi.org/10.5281/zenodo.10567648
Experimental models: Organisms/strains		
Mouse: *ArpC4*$^{flox/flox}$	van der Kammen et al.[18]	N/A
Mouse: B6.FVB-Tg(Zp3-cre)3Mrt/J	The Jackson Laboratory	RRID:IMSR_JAX:003394
Mouse: *Fmn2*$^{-/-}$	Leader et al.[59]	N/A
Oligonucleotides		
RT-PCR Primer for arpc4 ex1-3 forward: GGCTGCGCCTCTCTCGAAA	This paper	N/A
RT-PCR Primer for arpc4 ex1-3 reverse: CTTCACAGCAATGCTGACCC	This paper	N/A
RT-PCR Primer for arpc4 ex2-3 forward: ACCTTAGTGCCGTGCGGG	This paper	N/A
RT-PCR Primer for arpc4 ex2-3 reverse: CTTCACAGCAATGCTGACCC	This paper	N/A
RT-PCR Primer for actin forward: GGCTGTATTCCCCTCCATCG	This paper	N/A
RT-PCR Primer for actin reverse: CCAGTTGGTAACAATGCCATGT	This paper	N/A

(*Continued on next page*)

Please cite this article in press as: Nikalayevich et al., Aberrant cortex contractions impact mammalian oocyte quality, Developmental Cell (2024), https://doi.org/10.1016/j.devcel.2024.01.027

Continued

REAGENT or RESOURCE	SOURCE	IDENTIFIER
Recombinant DNA		
pspe3-GFP-UtrCH	Azoury et al.[31]	N/A
pCS2-Fmn2-Myc	Azoury et al.[43]	N/A
pRN3-Histone(H2B)-RFP	Tsurumi et al.[60]	N/A
pTALYM3-TALE- mClover-MajSat	Wu et al.[61]	N/A
pGMHE-eGFP-Rab27a	Cheeseman et al.[42]	N/A
Software and algorithms		
MetaMorph Version 7.7.9.0	Universal Imaging	N/A
Embryo Viewer	Vitrolife	N/A
Fiji	Schindelin et al.[62]	N/A
Fiji StackReg plugin	Thévenaz et al.[63]	N/A
Fiji TrackMate plugin	Tinevez et al.[64]	N/A
Fiji stics map jru v2 plugin	Jay Unruh at Stowers Institute for Medical Research in Kansas City, MO	N/A
Fiji Linear stack alignement with SIFT plugin	Lowe[65]	N/A
Fiji plugin Oocytor	Letort et al.[36] and this paper	https://github.com/gletort/Oocytor https://github.com/gletort/Oocytor/tree/main/models/cortex/retrainedOnHumans
Fiji Contour Curvature plugin	Bureau H. Glünder	https://www.gluender.de/Miscellanea/MiscTexts/UtilitiesText.html
Fiji Radioak plugin	This paper	https://zenodo.org/record/6854802 https://doi.org/10.5281/zenodo.6854802
Bundling score python package	This paper	https://github.com/VirtualEmbryo/bundling_score
Prism 9.0	GraphPad	N/A
MATLAB Version 2016a	MathWorks	N/A
MATLAB class MSDanalyzer	Tarantino et al.[66]	
Other		
recombinant hCG	Merck	Ovitrelle
triptoreline	Ipsen Pharma	Decapeptyl
Heparin-supplemented collection medium	Vitrolife	ASP
fertilization media	Origio	Sequential Fert
recombinant human hyaluronidase	Origio	ICSI Cumulase

RESOURCE AVAILABILITY

Lead contact

Further information and requests for resources and reagents should be directed to and will be fulfilled by the Lead Contact, Marie-Hélène Verlhac (marie-helene.verlhac@college-de-france.fr).

Materials availability

This study did not generate new unique reagents.

Data and code availability

- All data reported in this paper will be shared by the lead contact upon request.
- Python package for bundling score measurement and Fiji plugins generated in this study have been deposited on Github and Zenodo and are available as of the date of publication. Accession links are provided in the key resources table.
- Any additional information required to reanalyze the data reported in this paper is available from the lead contact upon request
- Table S1 can be found at this link: https://zenodo.org/records/10567648

Please cite this article in press as: Nikalayevich et al., Aberrant cortex contractions impact mammalian oocyte quality, Developmental Cell (2024), https://doi.org/10.1016/j.devcel.2024.01.027

EXPERIMENTAL MODEL AND STUDY PARTICIPANT DETAILS

Animal model

All animal studies were performed in accordance with the guidelines of the European Community and were approved by the French Ministry of Agriculture (authorization N°75–1170) and by the Direction Générale de la Recherche et de l'Innovation (DGRI; GMO agreement number DUO-5291). Animals were housed in the Center for Interdisciplinary Research in Biology (CIRB) animal facility. All mice used in this study were housed under standard laboratory conditions on a 12h light/dark cycle and received food and water *ad libitum*.

Human oocytes sources

The oocytes shown in Figures 4A–4C, S2F, and S2H were collected during assisted reproduction treatment in the Centre Assistance Médicale à la Procréation Nataliance (Groupe Mlab, Pôle Santé Oréliance, Saran, France). These oocytes have been donated to research (and discarded afterwards) as byproducts of the IVF procedure. The videos are anonymized and not related to the patient's data. According to the French Regulation regarding IVF, all patients gave informed consent to undergo the IVF procedure and signed a consent form where it is clearly stipulated that the IVF center can use anonymized data for training, quality control, internal research purpose as well as data transmission to the national IVF registry. Furthermore, according to the CNIL (French patient Data Protection Authority), anonymized videos of maturing human oocytes are not considered as health data or identifying data. This research is not intended to provide direct medical or financial benefit to anyone including the donor.

The oocytes shown in Figure S3D were acquired as part of a previous study.[47]

METHOD DETAILS

Mouse oocyte collection and culture

Ovaries were collected from 8-16-week-old females: control (wt/flox Cre-, wt/flox Cre+, flox/flox Cre-, wt/wt Cre+ or wt/wt Cre-), conditional knockout for ArpC4 (flox/flox Cre+), full knockout Fmn2 (*fmn2*$^{-/-}$)[59] or crosses of conditional knockout for ArpC4 with the full knockout Fmn2 (to produce *arpc4*$^{-/-}$*; fmn2*$^{-/-}$ oocytes). The Cre recombinase is expressed only in growing oocytes thanks to the ZP3 promoter. Oocytes were extracted and cultured in homemade M2 medium as described.[67] To keep the oocytes in prophase I arrest, the M2 medium was supplemented with 1 μM milrinone, and when needed the oocytes were permitted to exit prophase I arrest by milrinone washout.

Human prophase I oocytes collection, processing and culture

All prophase I oocytes were obtained from cumulus-oocyte complexes (COCs) harvested after controlled ovarian stimulation down-regulated with ganirelix (antagonist protocol). Ovulation and final oocyte maturation were triggered using 250 micrograms of recombinant hCG (Ovitrelle, Merck, Germany) and/or 0,2mg triptoreline (Decapeptyl, Ipsen Pharma, France). For agonist trigger cycles, luteinizing hormone (LH) was measured 12h after triptoreline injection and a new injection of 125 micrograms of rhCG was performed in less than 18h after the initial trigger if LH was inferior to 35 IU/mL. Follicular fluids were aspirated 36-38h post trigger in 14mL tubes filled with a Heparin-supplemented collection medium (ASP, Vitrolife, Sweden) kept at 36.5°C, using a 17-gauge single lumen aspiration needle (Cook Medical, Australia) and a negative aspiration pressure of 120mmHg. Follicular fluid screening was performed in an environmental chamber kept at 37°C and 6% CO_2 (Celltek 3000, Tek-event, Australia) using 60mm petri dishes (Vitrolife, Sweden). COCs were rinsed twice and trimmed in collection media (ASP, Vitrolife, Sweden), before being transferred into a holding dish (Universal GPS, LifeGlobal, USA) containing 100 μL microdrops of fertilization media (Sequential Fert, Origio, Denmark) under oil (Liquid Paraffin, Origio, Denmark) pre-equilibrated overnight at 37°C, 6.5% CO_2 and 5% O_2 in a BT37 incubator (Planner, UK). After 2 to 4 hours of incubation in a BT37 incubator, COCs were denuded in the environmental chamber using a 135 microns EZ-squeeze tip (Origio, Denmark) after a 1-minute exposure to 80U/mL recombinant human hyaluronidase (ICSI Cumulase, Origio). Denuded oocytes were then rinsed in multiple drops of Sequential Fert and transferred to the intracytoplasmic sperm injection (ICSI) dish where they were exposed to a MOPS buffered media at 36.5°C during the time of the ICSI (G-MOPS Plus, Vitrolife, Sweden). All metaphase II and metaphase I oocytes were injected during the ICSI process and all oocytes including prophase I were then rinsed in 4 microdrops of continuous embryo culture media (Sage One Step, Origio) before being transferred in the final incubation dish (Embryoslide Plus, Vitrolife, Sweden), containing Sage One Step under oil (Ovoil, Vitrolife, Sweden) pre-equilibrated overnight in the Embryoscope Plus Time-Lapse incubator (Vitrolife, Sweden) at 37°C, 6% CO_2, 5% O_2, 89% N_2. Undisturbed continuous culture was then performed in the same incubation conditions for a maximum of 8 days (Day 0 to Day 7).

The images and graphs in Figure S3D were generated through the analysis of videos from 46 live human oocytes that were acquired as part of a previous study.[47] The subset of cells included in these analyses was imaged continuously at fixed time intervals, underwent NEBD and progressed through meiosis until the MII stage. Time lapse videos of live human oocyte meiosis were analyzed using ZEN blue 3.0 software to determine the timing of meiotic progression and to score for cortical instability, spindle instability and multiple meiotic defects. Oocytes were assigned to the contracting or non-contracting group based on a visual inspection of the oocytes' surface dynamics in the transmitted light channel.

Please cite this article in press as: Nikalayevich et al., Aberrant cortex contractions impact mammalian oocyte quality, Developmental Cell (2024), https://doi.org/10.1016/j.devcel.2024.01.027

Human prophase I oocyte image acquisition

Videos of maturing prophase I oocytes were collected retrospectively using the Embryo Viewer software (Vitrolife, Sweden), after an initial adjustment of the video focal plane on the prophase I oocyte. Using the Embryoscope Plus incubator, images were acquired in 2048 x 1088 pixels (2.2 MP) with a 12-bit monochrome CMOS camera. A custom-made, high-quality 16x, 0.50 N.A. LWD Hoffman Modulation Contrast objective providing a resolution of 3 pixels per μm was used in conjunction with a single red LED for illumination (627 nm, duration $\leq$ 0.02 seconds per image). For each oocyte, the total light exposure time was < 40 seconds per day with a 10 minutes cycle time between image acquisitions.

RT-PCR

Total RNA was extracted from oocytes arrested in prophase I with the help of RNAqueous™-Micro Total RNA Isolation Kit (ThermoFisher #AM1931) and iScript™ Reverse Transcription Supermix (Bio-Rad #1708841) according to manufacturer's instructions. Primers: arpc4 ex1-3: GGCTGCGCCTCTCTCGAAA, CTTCACAGCAATGCTGACCC; arpc4 ex2-3: ACCTTAGTGCCGTG CGGG, CTTCACAGCAATGCTGACCC; actin: GGCTGTATTCCCCTCCATCG, CCAGTTGGTAACAATGCCATGT.

Immunoblotting and antibodies

Immunoblotting was conducted as described previously,[68] antibodies against ArpC4 (Everest Biotech #EB08249), ArpC2 (ProteinTech #15058-1-AP), Arp3 (Abcam #ab49671) and ERK-1 (Santa Cruz Biotechnology #sc-94) were diluted 1/1000 and anti-goat HRP-conjugated antibody (ThermoFisher #A16005) and anti-mouse HRP-conjugated antibody (Sigma #GENA931-1ML) were diluted 1/20000; anti-rabbit HRP-conjugated antibody (Sigma #GENA934-1ML) was diluted 1/10000 using SignalBoost™ Immunoreaction Enhancer Kit (Millipore #407207-1KIT). The staining was revealed with Thermo Scientific™ SuperSignal™ West Femto Maximum Sensitivity Substrate (Fisher Scientific #11859290).

Constructs, *in vitro* transcription of cRNA and microinjection

We used the following constructs: pspe3-GFP-UtrCH,[31] pCS2-Fmn2-Myc,[43] pRN3-Histone(H2B)-RFP,[60] pTALYM3-TALE-mClover-MajSat[61] (gift from Keith T. Jones, University of Adelaide, Australia), pGMHE-eGFP-Rab27a[42] (gift from M. Schuh). *In vitro* synthesis and oocyte microinjection of capped mRNA was done as described.[67] Final concentrations of cRNA for GFP-UtrCH were >800ng/μL (for cytoplasmic actin and cortical thickness measurements) or 200-400ng/μL (for cortical structure observation and bundling score quantification), for Fmn2-Myc was >800ng/μL, for GFP-Rab27a was 450 ng/μL.

Drug treatments

Oocytes were treated with 60 μM ML7 (Merck #I2764) in M2 medium for 2h. Metaphase II oocytes were treated with 200 μM monastrol (Sigma #M8515) for 2 h.

Live imaging

Spinning-disc microscope imaging was performed as described.[37]

Oocytes were placed in Fluorodish (World Precision Instruments #FD35–100) in small drops of M2 medium covered with mineral oil. Acquisitions were taken in transillumination in a single z slice with the time step of 1 minute (for cortex displacement quantifications) or 10 minutes (for PBE quantifications) for the duration between 1h and 12h.

For cortical structure observations during meiosis resumption, oocytes were microinjected with GFP-UtrCH mRNA, the oocytes were incubated for 10-20 min and released from prophase I arrest. The imaging started immediately after. The oocyte cortex was imaged every 2 min at 16 z-stacks with 1 μm step between stacks.

For cortical structure observations during meiosis I progression, z-stacks were imaged every hour until BD+6h.

For cortical granules observations, oocytes were microinjected with GFP-Rab27a mRNA, incubated for 4h and released from prophase I arrest. Imaging started immediately after the release on a single z slice with timepoints every hour until PBE.

For spindle morphology observations, the oocytes were incubated in M2 medium with 100nM Sir-Tubulin (Spirochrome #SC006) at 37°C for 1h and imaged from BD+4h every 30 min until anaphase at 8 z slices with a 4 μm step between stacks.

QUANTIFICATION AND STATISTICAL ANALYSIS

Spindle morphology measurements

Spindle morphology was observed in oocytes stained for tubulin at BD+4h and at the last timepoint before anaphase (30 min or less before anaphase). Only the oocytes with the spindle parallel to the imaging plane were considered. 3 z slices covering the spindle area were merged on a "Maximum Intensity" projection mode, then an ellipse was drawn around the spindle and major and minor axes were measured, corresponding to spindle length and width respectively.

Cortical thickness and F-actin in the cytoplasm

Cortical thickness was measured in oocytes expressing GFP-UtrCH probe at BD+8h on a z slice going through the widest part of the oocyte. Thickness was measured by manually placing lines perpendicularly to the cortex in 6 places. The average of these 6 measurements was the cortical thickness of a given oocyte.

Please cite this article in press as: Nikalayevich et al., Aberrant cortex contractions impact mammalian oocyte quality, Developmental Cell (2024), https://doi.org/10.1016/j.devcel.2024.01.027

Fluorescence intensity of F-actin the cytoplasm was measured in the same images by taking the mean fluorescence of the area taking most of the oocyte cytoplasm and removing background signal. The measurements were then normalized by the mean signal of control oocytes.

Cytoplasmic activity measurements

Nile red stain (Sigma, #N3013) was used to label the lipid particles. It was diluted at 5mg/ml in DMSO and stored at room temperature. It was diluted in M2 medium with a final concentration of 10 μg/ml and the oocytes were stained for 15 min at 37°C. To track the lipid particle movement, for each oocyte, a single z was taken every 500ms for 2min using Metamorph software (Universal Imaging, version 7.7.9.0) streaming acquisition mode. The resulting images were corrected for bleaching using histogram matching method and re-aligned with Fiji StackReg plugin.[63] Using TrackMate plugin[64] for Fiji,[62] particles were identified by thresholding and filtered for size (only particles between 0.4-1 μm^2 were analyzed). Tracks longer than 15 s were exported. Mean squared displacement (MSD) was calculated for each oocyte using MatLab class MSDanalyzer.[66] Diffusion coefficient was calculated considering the following formula: MSD = 4Dt (with t as the delay).

STICS measurements

To quantify the cytoplasmic movements by spatial temporal image correlation spectroscopy (STICS),[37,69] we used the plugins written for Fiji downloaded from (http://research.stowers.org/imagejplugins) and implemented for detecting cytoplasmic flows in mouse oocytes. We first aligned the transmitted-light movies of oocytes dividing in the plane of imaging using the "Linear Stack Alignement with SIFT" plugin in Fiji and we subtracted the moving average. We then ran "stics map jru v2". This plugin measures the velocity vectors of the cytoplasm from temporal and spatial correlation through the different timepoints of the movie, using a time correlation shift of 1. After running the plugin, we obtained STICS maps as well as an excel file with the numerical values of all the vectors. The STICS maps were normalized in order to obtain vectors of the same length, and their velocity intensities are represented by a color gradient. In order to put all images on the same color scale, we applied the same contrast and brightness settings to all images We then calculated the velocities using the coordinates of the vectors[70] given by the plugin to quantify the average cytoplasmic movement, but also in order to determine the highest one amongst our data set to establish the scale. Films for both controls and *arpc4*$^{-/-}$ were analyzed from BD+2h20 to BD+2h40.

Lipid particle volume

Oocytes stained with Nile Red dye were imaged on multiple z slices covering the whole oocyte, with 1 μm distance between slices. Each particle was identified by thresholding and their volume calculated based on areas in the neighboring z slices. The average volume of lipid particles was then calculated for each oocyte.

Mitochondria distribution

Oocytes at BD+2h or BD+6h were incubated in the M2 medium with 100 nM MitoTracker™ Red CMXRos (Thermofisher #M7512) for 30 min at 37°C, then imaged with a z stack covering the widest part of the oocyte with a 1 μm step between z slices. To analyze the distribution, 3 z slices of the widest part of the oocyte were merged on a "Maximum Intensity" projection mode. The mitochondria signal was manually thresholded, and regions of interest (ROI) larger than 12.9 μm^2 were analyzed. For each mitochondrial mass, the distance between the center of the mass and the center of the oocyte was calculated and normalized to the oocyte radius.

Mitochondria activity assay

Oocytes were incubated in the M2 medium with 25 nM TMRM dye (ThermoFisher #T668) for 30 min at 37°C, then imaged with a z stack covering the entire oocyte, with 4 μm step between z slices. To quantify the total fluorescence, all z slices were merged on a "Sum" projection mode, background signal removed and total signal of all the pixels in an image was measured. The measurements were normalized between experiments to the average values of the control oocytes.

Chromosome counting and measure of kinetochore distance between sister pairs in intact oocytes on monastrol spreads

Chromosome counting in live metaphase II oocytes was done as described.[17] The distance between pairs of sister chromatids was counted on the same images of live metaphase II oocytes by drawing a line (in Fiji) between the centers of MajSat-Clover signals on each chromatid in a pair. Only chromatid pairs parallel to the observation plane were measured.

Fertilization assay

Superovulation was induced by intraperitoneal injections of 5 units pregnant mare serum gonadotropin (Centravet #PMS005) and 5 units human chorionic gonadotropin (Centravet #CHO0003) 84h and 12h respectively prior to fertilization. Females were placed in cages with sole males overnight, then retrieved and sacrificed the next morning. Zygotes and unfertilized oocytes were collected from the ampulla in the fallopian tubes and counted, then stained with 10 μg/mL Hoechst 33342 (Thermofisher #H3570) in M2 medium for 15 min at 37°C and imaged on a spinning-disc microscope on planes covering the whole thickness of the zygote.

Please cite this article in press as: Nikalayevich et al., Aberrant cortex contractions impact mammalian oocyte quality, Developmental Cell (2024), https://doi.org/10.1016/j.devcel.2024.01.027

Fertility assay

Control or conditionally knocked out female mice were mated with wild type males for 6 months and the cumulative number of live birth pups was recorded.

Machine learning approach for mouse oocyte morphological characterization

Machine learning pipeline based on our open-source Fiji plugin Oocytor[36] (available in the GitHub repository https://github.com/gletort/Oocytor) to automatically measure and compare morphological features of control and *arpc4*$^{-/-}$ oocytes was used as described.[71] We aligned all the movies by their time of NEBD (manually annotated). Oocytor allowed us to automatically detect the oocytes contours and extract several features describing their morphology and dynamics[36] at each time point. To estimate Oocytor's discriminative power (i.e. Oocytor score, as seen in Figure 2A) during oocyte meiosis, we trained and tested a random forest classifier with a 5-fold cross validation scheme every 15 min. At each time point, we split the dataset (73 *arpc4*$^{-/-}$ oocytes, 64 control oocytes) in 5 groups. A random forest classifier was trained on 4/5 groups and we evaluated its performance on the fifth group by measuring the accuracy of the classification. This was repeated so that each of the 5 groups would be left out and used for testing once, so we obtained 5 scores for each time point.

In the first setup, all extracted features (104 features) were integrated in the pipeline to maximize the potential of discrimination of the pipeline. We measured the Gini index (feature importance to the classification) of each feature to highlight which features were the most relevant to the classification.[36,71]

In the second setup, we decided to test the discriminative power of the cytoplasmic features which were revealed as important in the first step. For this, we performed the same analysis but considering only cytoplasmic features (64 features, no cortical dynamics features) in the pipeline.

Machine learning approach for human oocyte movie analysis

Human oocytes were filmed in transmitted light in a clinical context over 160 h. As Oocytor was developed for meiosis I analysis only, we kept only the first 60 h of movies for analysis. Several wells contained more than one oocyte, so we separated the oocytes with a Fiji macro that automatically detected individual oocytes, so that each movie contained one centered oocyte. Movies were all aligned in time with the SIFT Fiji plugin.[65] Oocytor Fiji plugin[36] segmented oocyte contours (cortex and zona pellucida) by using neural networks based on the U-Net architecture. Initially, Oocytor's neural network performance was poor for these movies, especially for oocytes that touched the well boundary, as these were not represented in the training data. We thus retrained Oocytor networks on several images that were badly segmented. After a few retraining rounds, we obtained acceptable segmentation to use on the whole dataset. The retrained networks on human oocyte data are available in our github repository (https://github.com/gletort/Oocytor/tree/main/models/cortex/retrainedOnHumans). As a lot of oocytes were against the well boundary, their zona pellucida was often un-analyzable, so we focused our analysis solely on cortical and cytoplasmic features (71 features). We left out of the analysis a few oocytes that could not be properly segmented or analyzed. We processed 416 oocytes, with 114 not entering meiosis I, 47 not extruding a polar body and 255 undergoing a complete meiosis I. We checked that the timing of polar body extrusion was in the correct range for human oocytes (14-15 h), leaving us with 244 oocytes. Finally, we aligned the movies of oocytes entering meiosis relative to their timing of NEBD to be able to compare the features at similar developmental stages.

PIV from trans images

The Particle Image Velocity (PIV) was measured in mouse and in human oocyte time-lapse images with the Oocytor "Get PIV" feature based on the Particle Image Velocimetry Fiji plugin from Tseng et al. 2012.[72]

Curvature measurements

Oocyte outlines were segmented from transillumination images using the Oocytor "Get cortex" feature and local curvatures were measured with the "Contour Curvature" plugin for Fiji. The contour curvature was defined as 1/r where r is a radius of a circle that fits in the curved region. For display purposes, the curvatures between -0.0117 μm^{-1} (concave) and 0.0994 μm^{-1} (convex) were color-coded on a 0-254 grayscale and assigned color according to "Fire" look-up table in Fiji.

Radii change kymographs and cortex displacement speed measurements

Oocyte outlines were segmented from transillumination images using the Oocytor "Get cortex" feature. With the Radioak plugin for Fiji (https://zenodo.org/record/6854802) the radius was measured at 3.6° increments from the center of the oocyte, resulting in 100 radius measurements. This was repeated for each timepoint (at 1min step between timepoints). The minute-to-minute differences between radius values at the same angle were displayed on a color scale between -1.2 to 1.2 μm.

Cortex displacement per minute was calculated as an average of absolute values of minute-to-minute difference between radius values. Where appropriate, cortex displacement speed per hour ($\mu m/h$) is either a sum of cortex displacement per minute within one hour of observation or an extrapolation of cortex displacement per minute.

Amplitude of oocyte shape change

Oocyte outlines were segmented from transillumination images using the Oocytor "Get cortex" feature. Within one hour of observation aspect ratio for each timepoint (1 minute between timepoints) was measured for each oocyte. The amplitude of oocyte shape change is the standard deviation of these measurements.

Please cite this article in press as: Nikalayevich et al., Aberrant cortex contractions impact mammalian oocyte quality, Developmental Cell (2024), https://doi.org/10.1016/j.devcel.2024.01.027

Bundling score

Fiber orientation was extracted from the image intensity I(r) and its gradient ∇I. The local orientation of the fibers u(r) is expected to be orthogonal to gradient of intensity, or equivalently to a unit vector n defined as:

$$\mathbf{n} = \frac{\nabla \mathrm{I}}{\| \nabla \mathrm{I} \|}$$

Based on the local orientation of fibers, we define a nematic tensor Q which quantifies the local orientation of the fibers:

$$Q_{ij}(\boldsymbol{r}) = I(\boldsymbol{r})\left(u_i u_j - \frac{\delta ij}{2}\right) = I(\boldsymbol{r})\left(\frac{\delta ij}{2} - n_i n_j\right)$$

The advantage of the nematic order parameter Q is that it encodes the fiber orientation and the density of actin through the fluorescence signal amplitude $I(\boldsymbol{r})$.

To define a bundling score, we need to quantify the degree of alignment along spatial directions, which is well measured by the spatial correlations of Q. We therefore define a local correlation coefficient $C(\boldsymbol{r})$ ranging from -1 to 1 as follows:

$$C(\boldsymbol{r}) = \frac{\int Q_{ij}(\boldsymbol{r}')Q_{ij}(\boldsymbol{r}'+\boldsymbol{r})d^2\boldsymbol{r}'}{\int Q_{ij}^2(\boldsymbol{r}')d^2\boldsymbol{r}'}$$

A value of 1 for $C(\boldsymbol{r})$ means that orientations are completely correlated (bundle), while a value of -1 indicates that orientations are anti-correlated, and a value of 0 means that there is no correlation (isotropic orientation).

By integrating $C(\boldsymbol{r})$ over the whole image, one obtains an average spatial correlation coefficient for filament alignment, which we called the bundling score in the text:

$$A = \int C(\boldsymbol{r})d^2\boldsymbol{r}$$

Since information is available only in a certain window ($0 < x < Lx$, $0 < y < Ly$), exact correlations cannot be computed for all r. Therefore, to obtain sufficient information and reduce noise, one varies r_x and r_y between 0 and 20px.

The implementation of this method was done in Python, using scikit-image[73] and scipy.[74] The code is available as a python package on https://github.com/VirtualEmbryo/bundling_score.

The characteristic area (i.e. the bundling score) was calculated in pixel^2, and was multiplied by the square of spatial resolution to convert to μm^2. The analyzed images were maximum projections of several planes covering the bottom cortical part of the oocyte. All images were corrected for bleaching using histogram matching method in Fiji.

Statistical analysis

All statistical analysis was done using GraphPad Prism 9.0.

Paired and unpaired t-test, Mann-Whitney test and Wilcoxon matched-pairs signed rank test were used where appropriate.

Each experiment was performed with at least 3 independent repeats.

Image treatment and figure preparation

All images were treated in Fiji and Adobe Photoshop for linear adjustments of contrast and brightness levels to an entire image. Figures were prepared with Adobe Illustrator.